



# Historic Concrete and Masonry Assessment by the Air-Coupled Impact-Echo Method | 2012-04

Pennsylvania State University



National Park Service  
U.S. Department of the Interior

National Center for Preservation Technology and Training



# Final Report

Historic Concrete and Masonry Assessment  
by the Air-Coupled Impact-Echo Method

Thomas E. Boothby, Ph.D., P.E., R.A.  
Paul Kremer  
Nicole Trujillo  
Brian Riewestahl

Department of Architectural Engineering  
The Pennsylvania State University  
104 Engineering Unit A  
University Park, PA 16802

Prepared for:  
US Department of the Interior  
National Center for Preservation Technology and Training  
Natchitoches, LA  
Contract No.:

10 January 2012

# Table of Contents

List of Figures .....	2
List of Tables .....	4
Executive Summary .....	5
1. Introduction.....	7
1.1 Background of Present Project .....	7
1.2 Description of the Impact-Echo Method .....	7
1.3 Review of Major Literature related to this project .....	11
1.4 Objectives of the Current Project .....	13
1.5. Project Scope.....	13
1.5.1 Historic Preservation of Masonry and Concrete .....	13
1.5.2 Forms of Concrete and Masonry in Historic Structures .....	14
2. Experimental Work on Concrete Slabs: Description and Results .....	16
2.1 Laboratory Trials .....	16
2.1.1 Undefected Slabs .....	16
2.1.2 Defected Slabs .....	17
2.1.3 Analysis of Laboratory Results .....	19
2.2. Field Testing of Concrete Roof Slabs .....	26
2.2.1 In Situ Testing .....	29
2.2.2 Ex Situ Testing .....	31
2.3. Forensic Analysis of Concrete Roof Slabs.....	33
2.3.1 Analysis Approach .....	33
2.3.2 Slab Cut Locations .....	35
2.3.3 Results .....	36
3. Experimental Work on Masonry Walls: Description and Results.....	39
3. 1 Masonry Wall Specimens: Lab .....	39
3.1.1 Testing .....	41
3.1.2 Results .....	41
3.1.3 Bonding Classification .....	42
3.2 Field Tests of Masonry Walls .....	46
3.2.1 Field Test: Geisinger Medical Center .....	46
3.2.1.1 Testing .....	47
3.2.1.2 Results .....	51
4. Conclusions .....	52
4.1 Range of Applicability of ACIE.....	52
4.2 Special Instructions/Cautions in the Application of Air-Coupled Impact Echo .....	53
5. Acknowledgments .....	54
6. References Cited.....	55

## List of Figures

Figure 1.1: Typical time domain waveform .....	10
Figure 1.2: Typical frequency domain waveform .....	10
Figure 2.1: Frequency spectra with spring ball impactors at impact point 20 on slab .....	16
Figure 2.2: Frequency spectra with spring ball impactors at impact point 25 on slab .....	16
Figure 2.3: Frequency spectra with spring ball impactors at impact point 49 on slab .....	17
Figure 2.4: Defect locations and labels .....	17
Figure 2.5: Defect size and depth from top of slab .....	18
Figure 2.6: Testing grid layout on defected slab .....	19
Figure 2.7: Contour plot of defected slab from IEI scan with 3/8" impactor .....	21
Figure 2.8: Contour plot of defected slab from AIS prototype scan with 3/8" impactor .....	21
Figure 2.9: Contour plot of defected slab from AIS prototype scan with 5/8" impactor .....	22
Figure 2.10: Contour plot of defected slab from AIS prototype scan with 5/16" impactor .....	22
Figure 2.11: Contour plot of defected slab from AIS prototype scan w/ 5/16" impactor .....	23
Figure 2.12: Contour plot of defected slab from AIS prototype scan w/ 1/2" impactor .....	23
Figure 2.13: Example of a "clean" frequency spectrum from defected slab scan .....	25
Figure 2.14: Example of a frequency spectrum from defected slab scan .....	26
Figure 2.15: Layout of Section/Units .....	28
Figure 2.16: Single mat reinforcing and double mat reinforcing slab cross sections .....	29
Figure 2.17: In situ data contour plot of Section 1 Unit 3 with 5/8" impactor at 12" o.c. ....	30
Figure 2.18: In situ data contour plot of Section 3 Unit 1 with 7/16" impactor at 6" o.c. ....	31
Figure 2.19: Slab off-site storage support condition .....	31
Figure 2.20: Ex situ data contour plot of Section 1 Unit 3 with 3/8" impactor at 6" o.c. ....	32
Figure 2.21: Ex situ data contour plot of Section 3 Unit 1 with 3/8" impactor at 6" o.c. ....	33
Figure 2.22: Saw cutting of slabs ex situ .....	34
Figure 2.23: Saw cut locations on Section 1 Unit 3 .....	35
Figure 2.24: Saw cut locations on Section 3 Unit 1 .....	35
Figure 2.25: Cross section of Section 1 Unit 3 sub-unit A .....	36
Figure 2.26: Close up of cross section of Section 1 Unit 3 sub-unit A .....	36
Figure 2.27: Close up of differing concretes in cross section of Section 3 Unit 1 sub-unit C ....	37
Figure 2.28: Cross section of Section 3 Unit 1 sub-unit C between B and C .....	38
Figure 2.29: Cross section of Section 3 Unit 1 sub-unit C between C and D .....	38
Figure 3.1: Wall Specimen A1, A2 .....	39
Figure 3.2: Wall Specimen A.1 – Bond Disruption .....	39
Figure 3.3: Wall Specimen A.2 –Partially Filled Joints .....	40
Figure 3.4: Wall Specimen B1, B2 .....	40
Figure 3.7: Wall Specimen C.1, C.2, C.3, C.4 .....	40
Figure 3.8: Wall Specimen C.1 – Steel Beam and Wall Specimen C.2 – Terra Cotta Panel .....	40
Figure 3.9: Bonding Classification from Sadri (2003). .....	42
Figure 3.10: Wall Specimen A.1_Test 1Results .....	43
Figure 3.11: Wall Specimen A.1_Test 2 Results .....	43
Figure 3.12: Wall Specimen A.1_Test 3 Results .....	43
Figure 3.13: Wall Specimen A.2_Test 1Results .....	43
Figure 3.14: Wall Specimen A.2_Test 2 Results .....	43
Figure 3.15: Wall Specimen A.2_Test 3 Results .....	43
Figure 3.16: Wall Specimen B.1_Test 1Result .....	43

Figure 3.17: Wall Specimen B.1_Test 2 Results .....	43
Figure 3.18: Wall Specimen B.1_Test 3 Results .....	44
Figure 3.19: Wall Specimen B.2_Test 1Results .....	44
Figure 3.20: Wall Specimen B.2_Test 2 Results .....	44
Figure 3.21: Wall Specimen B.2_Test 3 Results .....	44
Figure 3.22: Wall Specimen C.1_Test 1Results .....	44
Figure 3.23: Wall Specimen C.1_Test 2 Results .....	44
Figure 3.24: Wall Specimen C.1_Test 3 Results .....	44
Figure 3.25: Wall Specimen C.2_Test 1Results .....	45
Figure 3.26: Wall Specimen C.2_Test 2 Results .....	45
Figure 3.27: Wall Specimen C.3_Test 1Results .....	45
Figure 3.28: Wall Specimen C.3_Test 2 Results .....	45
Figure 3.29: Wall Specimen C.3_Test 3 Results .....	45
Figure 3.30: Wall Specimen C.4_Test 1Results .....	45
Figure 3.31: Wall Specimen C.4_Test 2 Results .....	45
Figure 3.32: Test Location. ....	47
Figure 3.33: Removed brick at test site. ....	47
Figure 3.34: Wall tested: a) Lateral view. b) Wall Section. ....	47
Figure 3.35: Masonry Preservation Services Report Roof Level: a) Wall section. b &c) Photographs of old building before renovation. ....	48
Figure 3.36: Roof Level Wall with Relief Angles Testing Grid.....	49
Figure 3.37: Single Wythe 10-celled brick wall. ....	50
Figure 3.38: Impact echo response for single wythe 10-celled brick wall. ....	50
Figure 3.39: Geisinger Medical Center Test Results .....	51
Figure 3.40: Impact echo responses for points 1to 28. Peak 1 is at 2.5 kHz. Peak 2 is located at 7.1 kHz. ....	51

## List of Tables

Table 1.1: Acoustic impedances for different materials (Carino, 2011).....	9
Table 2.1: Intentionally placed defects in concrete slab .....	18
Table 2.2: Summary of scans performed on simple slab .....	19
Table 2.3: Summary scans performed on defected slab .....	20
Table 2.4: Approximate relationship of impactor size on key detection limits .....	24
Table 2.5: Classification of concrete slab test sections.....	27
Table 2.6: Physical dimensions of Units.....	28
Table 2.7: Summary of <i>in situ</i> testing performed .....	30
Table 2.8: Summary of <i>ex situ</i> testing performed.....	32
Table 3.1: Thickness frequency variables for triple-wythe wall.....	41
Table 3.2: Thickness frequency variables for single-wythe wall .....	49
Table 3.3: Thickness frequency variables for various wall construction.....	50

## Executive Summary

The impact-echo method is a non-destructive evaluation method in which internal pressure waves are excited through the thickness of a plate-like structure. By reviewing the frequency content of the internal reflections of the wave, the wave velocity can be inferred, and internal flaws, voids, and delaminations can be detected by interruptions of the wave propagation. The expected frequency of the reflections of an internal wave in an intact homogeneous material is known as the thickness frequency. Deviations from the thickness frequency are indicators of some sort of damage or defect in the internal structure. This method has been in use for over a decade as a means of non-destructive evaluation of concrete slabs and masonry walls. In the usual application of this method, a displacement transducer is put in positive contact with the surface of the structure under investigation, and the surface is struck with a hardened steel ball. This method presents some problems in surface preparation and in maintaining positive contact of the displacement transducer.

In the present project, the impact-echo method in a modified form is evaluated for use in the condition assessment of historic properties, particularly concrete slabs and masonry walls. The modification under investigation is known as the air-coupled impact echo method, in which the displacement transducer is replaced by a microphone held 1-2 cm from the surface within an acoustically isolated enclosure. The surface is struck by a hardened steel ball as close to the microphone as practicable, and the internal reflections of the pressure waves within the wall or slab are detected as acoustic input to the microphone. In this project, the air-coupled impact-echo method was tested in the laboratory and in the field on specimens of concrete slab and masonry wall.

The laboratory concrete slab specimens included intentionally cast-in defects, of different sizes and at different depths, and the ability of the system to detect these defects was examined. The fundamental frequency was recorded over a grid of test points superimposed on the specimen, and colored contour plots of this frequency were developed. The contour plots were very effective in indicating the locations of the defects: in general a significantly higher frequency than the thickness frequency was found at deep defects, while a lower frequency was recorded at shallow defects (replicating delaminations of the concrete cover). The system was tested in the field on reinforced concrete slab utility tunnel covers, that exhibited a variety of defects. These slabs were tested *in situ* immediately before removal for a reconstruction project, and on a remote site after their removal. Testing was done on a grid overlain on the slabs. Both testing programs indicated the presence of defects in some of the slabs. The presence of significant defects within the slabs was verified by saw-cutting the slabs and observing the defects directly.

The laboratory masonry specimens were built as 6 foot square two-wythe brick walls. In addition to a control specimen, the walls included intentional defects such as unfilled collar joints, steel inclusions, and disrupted bond. The walls were subjected to a testing program and the results of each test point were compared to a standard set of waveforms correlated to masonry defects, such as poor bonding, honeycombing, or very poor bonding. Based on these results, a plot of the wall was prepared, which was effective in locating the regions of internal defects in the walls. A similar program was undertaken in the field on a 1950's hospital building

undergoing selective replacement of its brick veneer wall. The system was also tried on a number of other historic buildings and structures.

It was concluded that the air-coupled impact-echo method is a promising alternative to displacement based impact echo analysis. In laboratory and field trials, the system was very effective in locating areas where invisible defects were present. The application of a microphone enclosure is significantly easier than a spring-loaded displacement transducer: it can be left on a horizontal surface, and needs minimum pressure to hold to a vertical surface. The frequency plot of the acoustic signal is easy to read, containing very distinct peaks in the frequency response. The system is applicable to concrete slabs between 2" and 18" in thickness

# 1. Introduction

## 1.1 Background of Present Project

Although the impact echo method has evolved into a standard method for the investigation of relatively shallow defects in concrete and masonry, it can still be cumbersome to apply, and the results can be difficult to interpret. The principal difficulty in application is the need to maintain a constant positive contact between the displacement transducer and the surface under investigation. This coupling is usually accomplished through a lead foil that wears out quickly. The results are obtained in the form of a waveform that is often difficult to interpret, and requires specific training of the operator in order for the method to be useful.

It is considered that the application of an alternative method, in which the signal from the structure is captured with a microphone instead of a displacement transducer may result in easier application and more reliable results. In the present study, the air-coupled impact echo system is applied to a number of historic and non-historic structures, including a collection of damaged concrete slabs, a number of brick wall specimens, and two load-bearing brick masonry buildings from the nineteenth century.

## 1.2 Description of the Impact-Echo Method

The impact-echo method involves the investigation and manipulation of stress waves, known as P-waves set up in a medium by a small impact. P-waves are stress waves comprised of zones of compressions and rarefactions. The most common example of this type of wave is a sound wave. The distinguishing feature of a P-wave is the fact that the material is stressed in the same direction that the wave is traveling. Directly after an impact event, the concrete or masonry directly under the impact location compresses in response to the force applied from the impactor. This compression continues through the concrete until it encounters a material with a different set of acoustic properties. The resulting wave consists of zones of compression and tension. While the energy of this wave is quickly dissipated, it can be captured by modern signal acquisition and processing equipment.

R-waves differ from P- and S-waves in that while P-waves and S-waves travel through the solid body, R-waves travel only along the surface of the solid. Even though it is the slowest of the three types of waves, the R-wave can provide important information about the impact and frequency content resulting from that impact (Sansalone and Streett, 1997). The most important piece of information an R-wave describes in the IE method is the contact time between the impactor and the substrate. When the contact time is known, the maximum usable frequency excited by that impact may be calculated by utilizing the following equations developed by Sansalone and Streett (1997):

$$t_c = .0043D \quad (\text{Eq. 1.1})$$

$$f_{max} = \frac{291}{D} \quad (\text{Eq. 1.2})$$

Where:

$t_c$  = contact time (s)  
 $D$  = diameter (m)  
 $f_{max}$  = maximum frequency of useful energy (Hz)

Contact time is linearly related to the diameter of the impactor, which is inversely related to the maximum frequency. Thus, as impactor diameter decreases, contact time decreases and maximum frequency increases. However, 3mm has been shown in practice to be the smallest useful size of impactor due to the appearance of higher frequencies that are easily attenuated by the natural discontinuities within the concrete matrix (Sansalone and Streett, 1997).

For an elastic solid in response to an impact event, and as such, P-wave velocities are functions of the modulus of elasticity, density, and Poisson's ratio (Sansalone and Streett, 1997).

$$C_p = \sqrt{\frac{E(1-\nu)}{\rho(1-\nu)(1-2\nu)}} \quad (\text{Eq. 1.3})$$

Where:

$C_p$  = P-wave velocity (m/s)  
 $E$  = Young's modulus (Pa)  
 $\nu$  = Poisson's ratio  
 $\rho$  = density (kg/m<sup>3</sup>)

However, since concrete is actually a heterogeneous material with material properties that vary even from batch to batch, items such as Poisson's ratio and Young's modulus are very rarely known with exact certainty. The result of this is that P-wave velocity needs to be measured on each tested concrete slab. The IE method relies upon the use of sensors that detect the P-wave reflections, so the sensors are placed next to the impact point to maximize the effect of P-waves and minimize those of other waveforms. (Sansalone and Streett, 1997).

The repeated reflections set up a type of resonance within the concrete slab and the multiple reflections of those waves make flaw detection possible in the IE method. The reflections of the stress wave are set up when the wave encounter materials of different acoustic properties. The key material property is called acoustic impedance, or  $Z$ , and the interaction of the stress wave at a boundary with materials of differing acoustic impedances, referred to as the reflection coefficient,  $R$ , is what gives rise to the reflections of the stress wave (Carino, 2011)(Krautkrämer and Krautkrämer, 1990). The reflection coefficient is defined as:

$$R = \frac{Z_2 - Z_1}{Z_2 + Z_1} \quad (\text{Eq. 1.4})$$

Where:

$R$  = reflection coefficient  
 $Z_1$  = acoustic impedance of material 1 (kg/m<sup>2</sup>s)  
 $Z_2$  = acoustic impedance of material 2 (kg/m<sup>2</sup>s)

When the stress wave hits one of these boundaries of materials the wave one of three consequences will occur: the energy will be reflected by the boundary, transmitted through the boundary, or a combination of those two in which some energy is reflected and some energy is transmitted. The amounts of energies reflected and transmitted are determined by the reflection coefficient for that particular boundary. Table 1.1 highlights the acoustic impedances materials that would typically be encountered in IE testing. In the scope of this work, the only types of material interfaces that are of interest are the concrete/air and concrete/steel boundaries.

Table 1.1: Acoustic impedances for different materials and reflection coefficients (Carino, 2011)

<b>Material</b>	<b>Specific Acoustic impedance, kg/(m<sup>2</sup>s)</b>	<b>Reflection coefficient at interface</b>
Air	0.4	-1.00
Water	1.48 * 10 <sup>6</sup>	-0.65 to -0.75
Soil	0.3 to 4 * 10 <sup>6</sup>	-0.3 to -0.9
Concrete	7 to 10 * 10 <sup>6</sup>	N/A
Steel	47 * 10 <sup>6</sup>	0.65 to 0.75

The concrete/air interface is the most common type of interface in IE (Sansalone and Streett, 1997). In this case, the  $Z$  of air is significantly smaller than the  $Z$  of concrete; this causes the majority of the stress wave's energy to be reflected back into the concrete with a phase change. For example the compression wave changes into a tension wave after reflecting off the boundary. This is shown as a reflection coefficient with a negative sign in Table 1.1. In the case of the concrete/steel interface, the  $Z$  of steel is greater than the  $Z$  of concrete, but not on the same order of magnitude as the concrete/air interface. In this case, part of the stress wave reflects back into the concrete without a phase change, shown by a reflection coefficient with a positive sign in Table 1.1, while the rest of the wave travels into the steel reinforcing bar. This occurs again, on the other side of the reinforcement as the wave goes through the steel/concrete interface. Once the stress wave is back into the concrete, it hits the concrete/air interface on the far side of the slab.

The stress wave in the concrete slab is governed by a relationship between velocity, frequency and wavelength.

$$C = f\lambda \quad (\text{Eq. 1.5})$$

Where:

$C$  = wave velocity (m/s)

$f$  = frequency (Hz)

$\lambda$  = wavelength (m)

Given a typical P-wave velocity of 4000 m/s for concrete, the frequency and wavelength become critical in the detection of internal flaws in the concrete (Sansalone and Streett, 1997). In order for a particle to be detected by an IE system, the wavelength of the stress wave must be smaller than the dimension of the object trying to be located. If the wavelength of the stress wave is larger than the object to be detected, the stress wave will "propagate through an equivalent

continuum whose properties combine the properties of the host medium and the inclusion” (Santamarina, Klein, and Fam, 2001). The goal of IE is to use a range of frequencies and wavelengths that are larger than the individual particles of the concrete matrix, but smaller than the dimensions of the flaws one is trying to detect. The range of frequencies typically utilized in IE range from 0 to 80 kHz (Sansalone and Streett, 1997).

The IE method relies upon the gathering of frequency and wavelength data in order to detect flaws in concrete. For a digital computer to acquire this type of information, it first must collect it over a finite period of time. This data is referred to a time domain data since it is a measure of the amplitude of the sounds versus the length of time it was collected in. Figure 1.1 shows a typical time domain waveform. In order to make sense of the digitalized data, the data needs to be transformed to the frequency domain, which is amplitude plotted against frequency. Figure 1.2 shows the previous time domain data transformed into a frequency domain waveform.

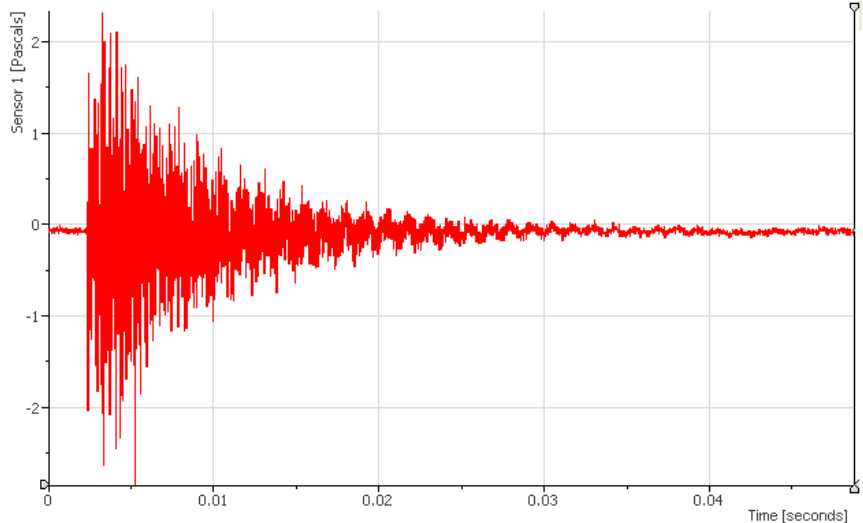


Figure 1.1: Typical time domain waveform

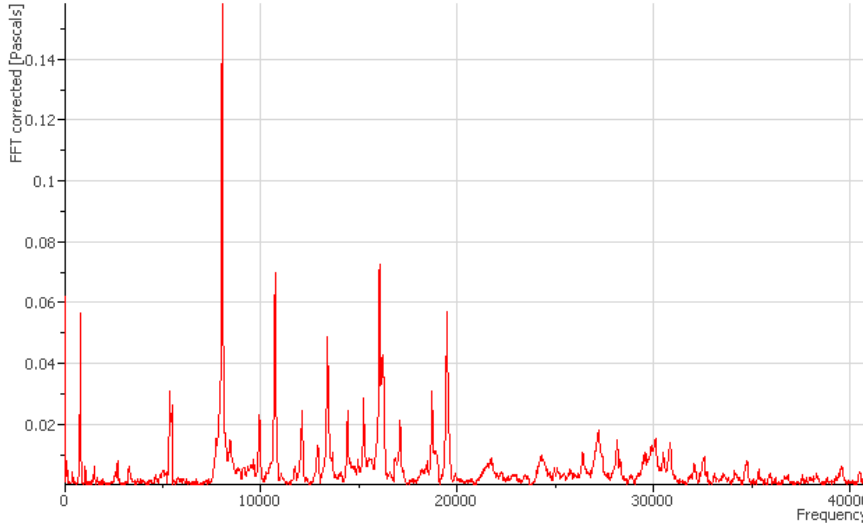


Figure 1.2: Typical frequency domain waveform

### 1.3 Review of Major Literature related to this project

The roots of the impact-echo method can be traced to its development in 1983 at the National Bureau of Standards (NBS) by Dr. Nicholas Carino and graduate student, Mary Sansalone (Sansalone and Streett, 1997). Early key innovations noted by Sansalone and Streett that made the full development of impact-echo include: use of finite element computer simulations to accurately model stress waves in a plate, generating stress waves from elastic impacts, development of a displacement transducer, and analysis of the signal in the frequency domain. In further research performed under Sansalone during her tenure at Cornell University, additional studies by her investigated the use of impact-echo for the evaluation of concrete elements with different cross sections and the effect of different types of flaws on the impact-echo signal in those elements, along with other permutations including reinforcing and differing material layers.

Sansalone and Streett also examined the development of the basic equations of the impact-echo method. Starting from a base of elastic stress waves in materials, they worked through the material mechanics (by treating concrete as a homogeneous material) to arrive at the core equations in the IE method:

$$f = \frac{\beta C_p}{2T} \quad (\text{Eq. 1.6a})$$

$$T = \frac{\beta C_p}{2f} \quad (\text{Eq. 1.6b})$$

Where:

$f$  = frequency (Hz)

$\beta$  = shape factor (.96 for plates)

$C_p$  = P-wave velocity (m/s)

$T$  = thickness (m)

The shape factor ( $\beta$ ) in Equation 1.6a and 1.6b was introduced into the equation as a means of reconciling the proposed equation to what was actually being measured in their experiments. This factor takes into account the nature of the first mode of vibration of the plate and varies for structural elements of differing cross sections. However, the shape factor was purely empirical at this stage of development of the IE method. A rationale for this shape factor was found by Gibson and Popovics (2005).

ASTM C1383(04) is the latest standard for testing using the impact-echo method. The standard procedures for determining P-wave velocity in a concrete slab and for performing an impact-echo test are covered and delineated. The previous work by Sansalone and Streett (1997) with surface-coupled sensors, served as the foundation for the first and subsequent drafts of this standard. Although the standard is based on surface-coupled sensors, the procedures are assumed to be reasonably valid for air-coupled sensors used in this project as well. The procedures covered in the standard were used as a guideline for the *in situ* and *ex situ* field testing. The standard also covers systematic errors inherent to the testing setup.

The use of air-coupled sensors is highly advantageous over the use of surface-coupled sensors because minimal time is required to prepare the concrete surface. Because the time-consuming process of grinding a rough concrete surface until it is smooth has been eliminated from the NDE process, the ACIE method is a much more attractive option for a preliminary inspection of a concrete slab. Zhu and Popovics (2005) explored the use of using air-coupled sensors for non-contact testing for surface cracks in concrete slabs. The basis of this exploration is the use of microphones to detect changes in air pressure above the slab instead of surface transducers that detect small displacements in the slab itself. The authors built upon their previous work (2001) that developed five key points:

- (a) air-coupled transducers may be used to detect the leaky surface waves or guided waves propagating in concrete;
- (b) air-coupled transducers are sensitive and tests can be performed over large distances up to 10 m, which is valuable for rapid scanning of large-scale structures;
- (c) the signals collected by air-coupled transducers have high S/N ratio even after propagation over large distances;
- (d) the highly directional feature of the microphone used in this research notably reduces the effect of the direct acoustic wave and ambient noise;
- (e) for thin slab and plate structures the detected leaky waves propagate as dispersive Lamb waves, and for thick structures as Rayleigh waves.

Building upon these principles, Zhu and Popovics set about testing the effect of surface cracks on both wave velocity and attenuation. Testing consisted of a mechanical impact and a series of three directional microphones fixed in a linear position at a set height and spacing, striking a surface and measuring the resulting surface wave velocity and energy between the microphone locations. Scans were carried out in a linear fashion in both the x and y axes, and then by combining the x and y scans, a 2-D image of the slab could be formed. The end results of the experiment were that air-coupled microphones could be used to locate surface cracks via the attenuation of the leaky surface waves across the cracks. However, depth of the crack could not be determined.

Berriman, Hutchins, et al. (2006) examined the use of different time-frequency analysis methods to accurately locate a piece of rebar in a concrete plate. An ultrasonic “chirp” signal ranging from 150 kHz to 650 kHz, along with some random noise, was put into the concrete plate at the focus of this experiment. The use of an ultrasonic “chirp” signal in the heterogeneous concrete provided noisy signals in the experiment.

Zhu and Popovics (2007) applied air-coupled sensors with the IE method for NDE of concrete slabs. They built upon previous work and not only tested on concrete slabs with internal defects, but also developed a unique microphone enclosure that blocks outside noise, allowing just the leaky surface wave information to be detected by the microphone.

The microphone enclosure derived by Zhu and Popovics was recreated by Boothby et al. (2010), and was used over the course of the work performed in this study. The enclosure consisted of four parts: the microphone itself, sound-blocking foam on the exterior, the aluminum cylinder

that provides the structure of the enclosure, and an inner layer of rubber to absorb the energy from the leaky waves, which prevents resonance of the waves forming inside the enclosure.

Zhu and Popovics tested a 1.5×2.0×.25m concrete slab with reinforcing and intentionally placed defects. The reinforcing consisted of #4 bars at 500mm on center (o.c.), along with 150×150mm wire mesh placed with 60mm of cover. The intentional defects placed in the slab consisted of layered plastic sheets and foam blocks to represent delaminations and internal voids. The results of the experiments carried out by Zhu and Popovics demonstrate that the use of the ACIE method for detecting internal flaws in a concrete slab is feasible and represents a promising line of continued study into the use of air-coupled sensors in the IE method for performing NDE of structural elements.

#### **1.4 Objectives of the Current Project**

The primary objective of the current project is to evaluate the applicability of the air-coupled method of impact-echo analysis to the assessment of historic concrete and masonry structures. A secondary objective is the refinement of the apparatus used in this testing to improve its portability and effectiveness, and eventually to make it suitable for use by a single operator.

Certain objectives apply to any system developed for non-destructive evaluation (NDE) of any structure. These include transparency and ease of operation, the ability to discriminate defects within a given range of size and depth, and the reliability of identifying and locating hidden defects *in situ*, and of avoiding false positives. Beyond the general objectives for the development of any system of NDE and its application to structures in concrete and masonry, some additional objectives apply to the assessment of historic concrete and masonry structures. These relate generally to the need to preserve these structures as much as possible. Because repairs to the structure generally involve removal of historic fabric, it is critically important to avoid false positive readings in a system designed for NDE for historic structures. The system needs to be able to discriminate defects from background noise in structures that are assembled with larger voids and greater initial variations in the material used. For instance, in a historic load-bearing masonry building, it may be necessary to take readings of multi-wythe load bearing brick walls with random header locations and with unfilled collar joints. Hence, a system proposed for use in historic brick masonry structures needs to discriminate between the complexities of ordinary construction and genuine defects within the structure.

#### **1.5. Project Scope**

**1.5.1 Historic Preservation of Masonry and Concrete:** Effective preservation of historic concrete and masonry structures requires significant attention to the condition of materials and assemblies in concrete and masonry. First, the simple preservation of the integrity of a structure requires that the owner and their consultants be aware of the condition and integrity of components such as masonry walls and concrete floor and roof slabs. Second, when the condition of these components is observed to require attention, the type and degree of intervention necessary must be assessed before undertaking repairs of any type. Third, the Secretary of the Interior's *Standards for the Treatment of Historic Properties* require a minimum level of intervention, and further require that existing fabric be repaired in place, rather than

replaced in any responsive repair to a historic property. This means that some form of non-destructive evaluation is necessary in order to determine the nature, the location, and the level of any interventions to a historic structure constructed of masonry or concrete. The objective of this project, as outlined above, is to assist in the development of a non-destructive evaluation procedure that can help in the identification and in the assessment of structural defects in historic structures.

The scope of this project is generally to investigate the air-coupled impact-echo method of non-destructive evaluation to determine its suitability as a non-destructive evaluation method, capable of determining the location, depth, and nature of concealed defects in a concrete floor system or a masonry wall. With this in mind, the following section will review the frequently recurring types of defects in such structures.

**1.5.2 Forms of Concrete and Masonry in Historic Structures:** The most frequent applications of concrete in historic structures are in walls and slabs. Slabs may also be supported by beams and columns, usually cast monolithically with the slab. One way slabs span from 2 feet (between joists) to 20 feet (between walls) with corresponding variations in thickness from 2-3" to 10-12". Slabs may also span two ways supported by columns in roughly square bays. Two way slabs have thickness from about 6" to 12". Reinforced concrete walls range in thickness from 6" to 24". They are often found on lower levels of buildings or used for basement walls. Concrete columns have dimensions ranging from 12" to 30" or larger.

Masonry is most frequently used as a material for the construction of walls, either load-bearing or non-load bearing. It was used universally as the material for creating enduring wall structures from the founding of the US through about the 1920's, when concrete began to make an appearance as a material for the construction of walls. The most common form of masonry wall is a multi-wythe brick wall. Around the turn of the twentieth century, however, brick began to be used as a veneer material supported by a wood structure. Concrete block also appears in the twentieth century, while stone or clay tile get occasional use in the nineteenth and early twentieth centuries. The construction of these walls is also varied, in that header courses are sometimes inserted, occasionally not, collar joints are often left unfilled, but sometimes filled hollow, frogged, or solid bricks may be used. The variety of brick types and mortar types must also be considered. Some brick are hand-molded and half fired, and have great variety in the stiffness of the material and in its density, both important parameters for the testing that will be described. Masonry tile is also used as a material for floors, or for creating vaulted and domed structures. The Guastavino system of constructing vaults with 6 × 12 × 1 inch tiles, laid flat in 3-5 or more layers is well-known as a means of achieving significant spans in load-bearing masonry construction. Various commercial fireproof floor systems, using special tile shapes, are also widespread throughout commercial buildings in the US.

Condition assessment is critical to all of these structure types. In horizontal structures, such as slabs or vaults, it is critical to detect the presence of voids, breaks or delaminations that may eventually compromise the load-carrying capacity of the system. In wall structures, it is important to have some idea of the extent to which the wythes of the wall remain bonded, and to determine the voids present from the original construction, and cracks or voids that may result from ongoing processes in the wall.

The principal defects in to be considered in concrete structures are:

Slabs:

Delamination—separation of the concrete cover over the top layer of reinforcement

Voids

Reinforcement corrosion

Beams:

Voids

Areas of segregation (in concrete placed without proper controls, the cement paste becomes separated from the coarse aggregate, resulting in internal rock pockets, surface honeycombing, or other areas of segregation).

Cracking: structural

Cracking: thermal, freeze-thaw, environmental

Reinforcement corrosion

Columns:

Segregation

cracking

Walls:

Segregation

Cold joints

Environmental damage

Reinforcement corrosion

The principal defects in masonry structures are:

Brick masonry (load bearing):

Lack of bond between wythes

cracking

environmental deterioration of masonry units.

Brick masonry (veneer):

Most problems visible to inspection

Concrete masonry:

Cracks

General deterioration

Reinforcement anchorage

# 2. Experimental Work on Concrete Slabs: Description and Results

## 2.1 Laboratory Trials

**2.1.1 Undeformed Slabs:** Initial testing of the system was done on a slab free of intentional defects. The defect-free slab scanned was an unreinforced, 48"×48"×5" slab resting on four concrete masonry unit blocks to provide a large concrete/air interface at the bottom of the slab. The tests included direct comparison of the ACIE system with a commercial IE system, and investigations of the use of varying sizes of spring balls. IE scanning of the undefected slab was conducted using the ACIE method, with a total of two scans performed. Both scans used the air-coupled microphones and software developed for the AIS prototype. A 3/8" diameter impactor was used in both scans and the software was set up to record 500 samples at a sampling frequency of 51200 Hz.

Frequency spectra from both of the scans performed were analyzed and compared to each other for each point impacted during the scan. Figure 3.1 through 3.3 show the frequency spectra from the spring ball at three different impact locations.



Figure 2.1: Frequency spectra with spring ball impactors at impact point 20 on undefected slab

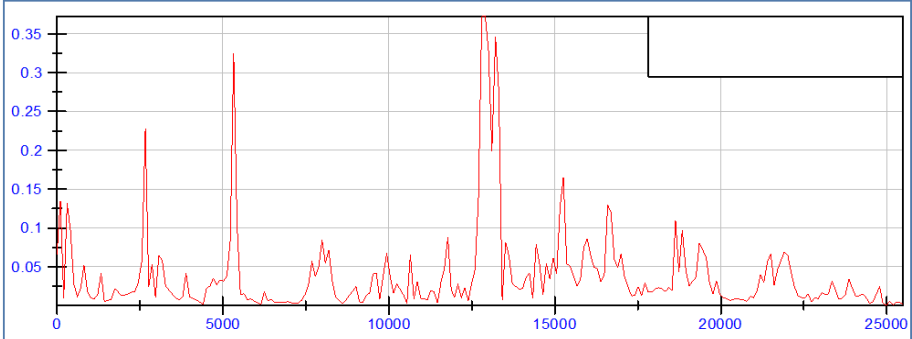


Figure 2.2: Frequency spectra with spring ball impactors at impact point 25 on undefected slab



Figure 2.3: Frequency spectra with spring ball impactors at impact point 49 on undefected slab

Frequency peaks at impact point 20 were at 12902 Hz. At impact point 25, the frequency peak was at 12902 Hz. At impact point 49, the peak was at a frequency of 13209 Hz. The approximate average thickness frequency of 13 kHz results in an estimate of the P-wave velocity of 3400 m/s. The lower frequencies are considered to result from reflections from the sides of the slab.

**2.1.2 Defected Slabs** The second slab scanned was a reinforced 60×80×10” slab resting on a wood frame support system. This slab was modeled after the intentionally defected slab used by Zhu and Popovics (2007). This slab’s reinforcing was placed in both a top and bottom layer comprised of 6×6” wire mesh and #4 bars spaced at 16” o.c. along the long axis of the slab and at 20” o.c. along the length of the short axis with 2” cover. In addition to the two layers of reinforcing, nine intentionally defected areas were cast into the slab as well. The placement and type of defects are given in Figure 3.4, Figure 3.5, and Table 3.1.

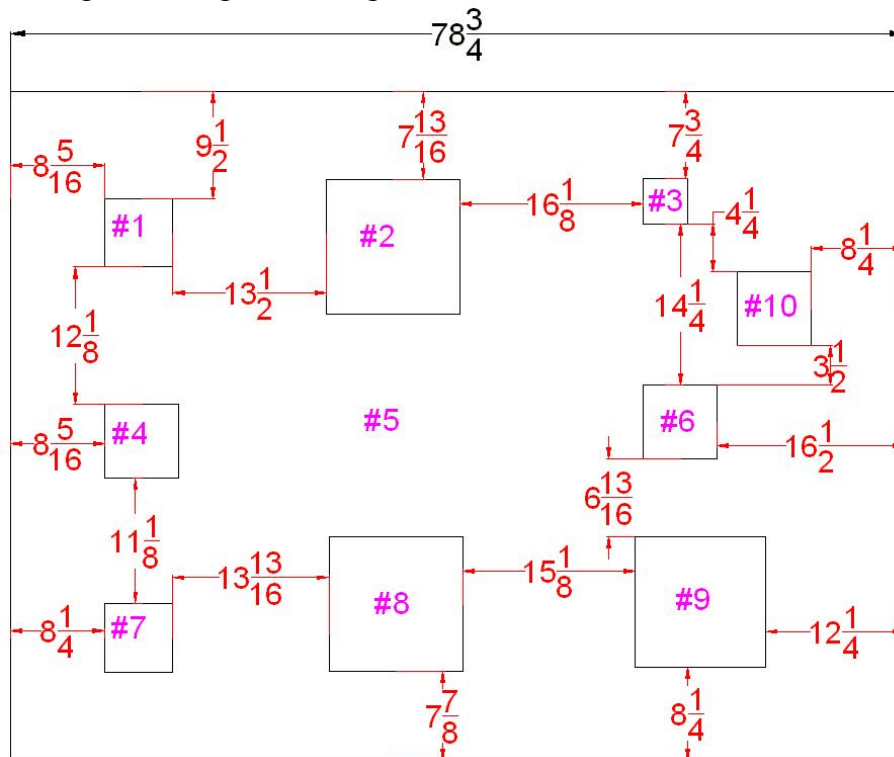


Figure 2.4: Defect locations and labels

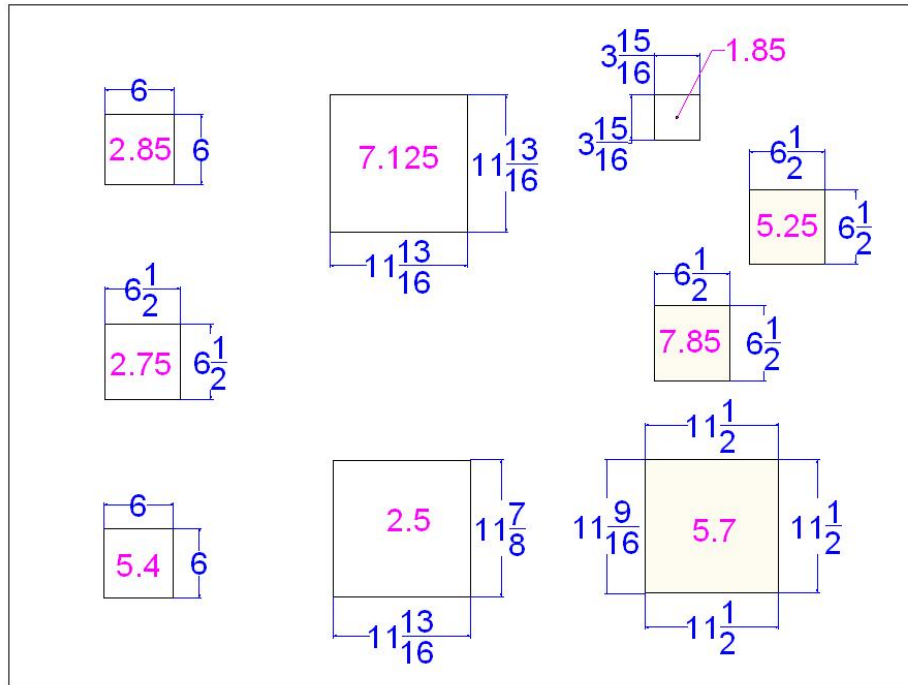


Figure 2.5: Defect size and depth from top of slab

Table 2.1: Intentionally placed defects in concrete slab

Defect	Type
1	Rock Pocket
2	Delamination
3	Delamination
4	Foam Block
5	No Defect
6	Rock Pocket
7	Rock Pocket
8	Delamination
9	Rock Pocket
10	Foam Block

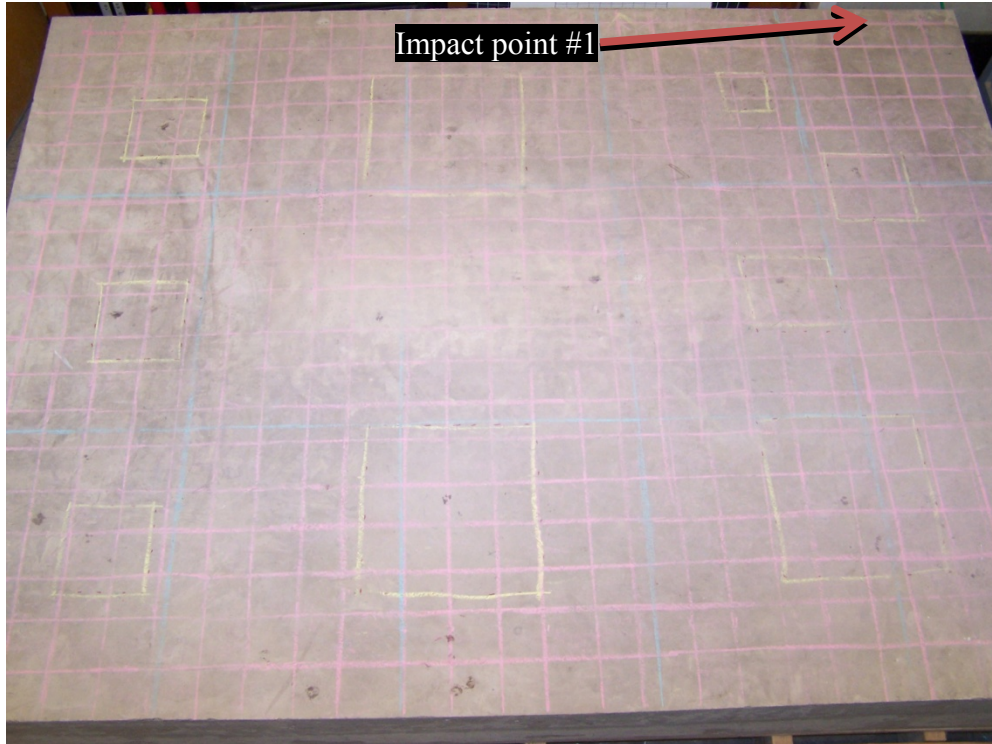


Figure 2.6: Testing grid layout on defected slab

**2.1.3 Analysis of Laboratory Results.** To establish the validity of the methods used, the results gained from the prototype were compared to results from a commercially available impact-echo system. The most widely used commercial impact-echo system, the IEI system, uses a piezoelectric transducer that is put in contact with the concrete surface. After scanning with the IEI system, the slab was then scanned using the ACIE system. The scans were conducted using a 3/8" diameter impactor. The data acquisition rate was set at 51200 Hz and a total of 500 samples were taken. The resulting frequency resolution of the scan was 102.4 Hz. The sampling rate and number of samples were set at these levels to try to minimize the effects of reflected waves due to the thin and relatively small overall size of the slab of the on signal quality. Results from other attempts with larger numbers of samples and a higher sampling rate were scattered and inconclusive due to multiple and unrepeatable peaks in the frequency spectrum.

The IEI system scan was performed using the same parameters as the ACIE scan, but variations were introduced into the ACIE scan. Variations included using different size impactors, different data acquisition rates, and different grid spacing.

Table 2.2: Summary of scans performed on simple slab

Impactor Diameter (in.)	Grid Size (in.)	Data Acquisition Rate (Hz)	Sample Size	Frequency Resolution (Hz)	Contour Plot Figure Number
3/8	6*6	500000	1024	490	--
3/8	6*6	51200	500	102.4	--

Table 2.3: Summary scans performed on defected slab

<b>Impactor Diameter (in.)</b>	<b>Grid Size (in.)</b>	<b>Data Acquisition Rate (Hz)</b>	<b>Sample Size</b>	<b>Frequency Resolution (Hz)</b>	<b>Contour Plot Figure Number</b>
3/8	6*6	1000000	1024	490	2.7
3/8	6*6	65536	2000	32.7	2.8
5/8	6*6	51200	2000	25.6	2.9
5/16	6*6	102400	2000	51.2	2.10
5/16	3*3	102400	1024	100	2.11
1/2	12*12	51200	2000	25.6	2.12

At the conclusion of each of the scans, a contour plot for the slab was generated in SigmaPlot software using the dominant frequency peak in the spectrum as the ‘z’ value in the plot, and ‘x’ and ‘y’ values represented the location of the impact on the slab. Areas around the edges of the slab were not able to be scanned in every test because of the physical limitations of placing the microphone enclosures at the edge of the slab, and due to unreadable signals due to reflections from the slab edge. These areas are marked as “No Data” and the location crosshatched.

During the course of testing on the simple slab with the IEI system, it was noticed that the small size and thickness of the slab resulted in increased noise in the signal gathered by the system. As a result of the data being “noisy” in much the same way as the early scans with the AIS prototype were, the data set sample number was increased from 1024 to 2048 and a filter on data below 5 kHz was added within the IEI software. Results from the scans performed on the defected slab with both the IEI system and the AIS prototype are shown in Figure 3.7 for the IEI system, and Figure 23.8 through 23.12 for the AIS prototype.

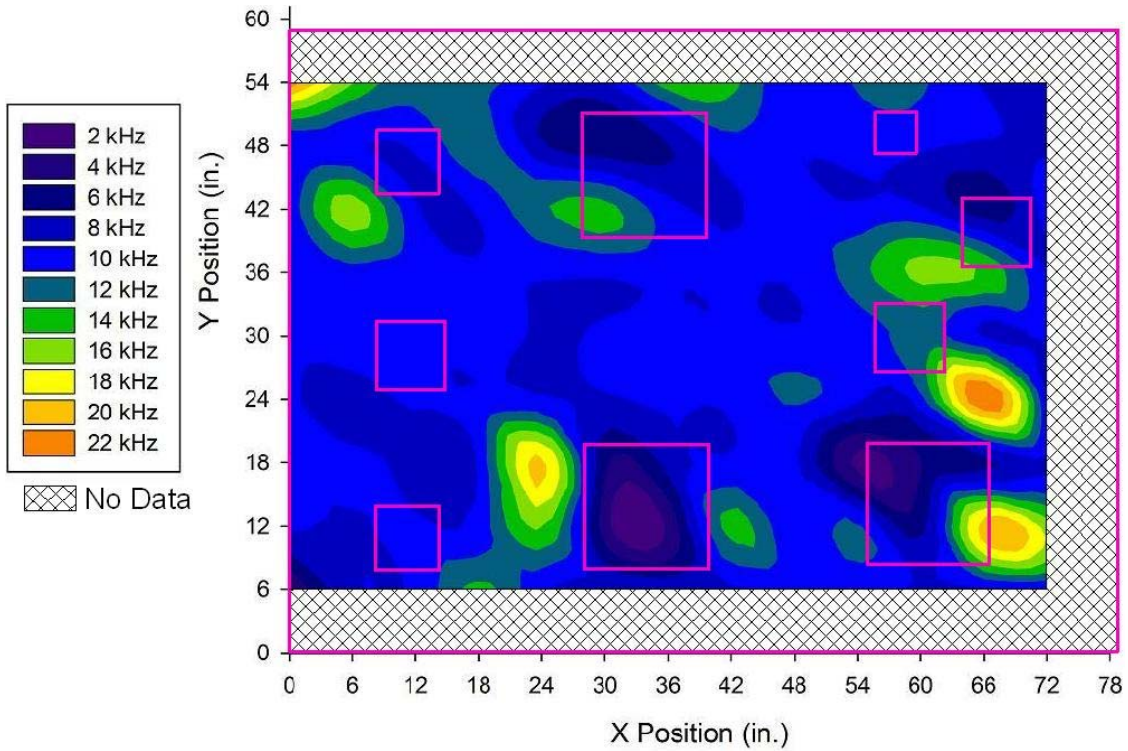


Figure 2.7: Contour plot of defected slab from IEI scan with 3/8" impactor at 6"o.c.

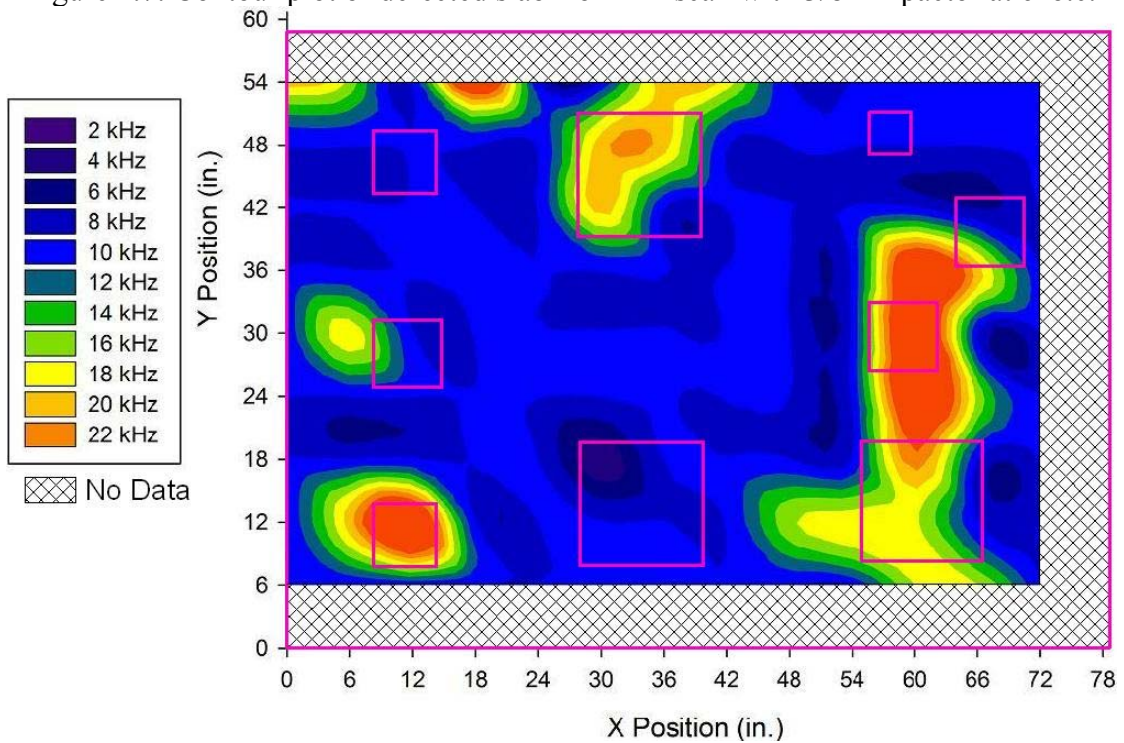


Figure 2.8: Contour plot of defected slab from AIS prototype scan with 3/8" impactor at 6"o.c.

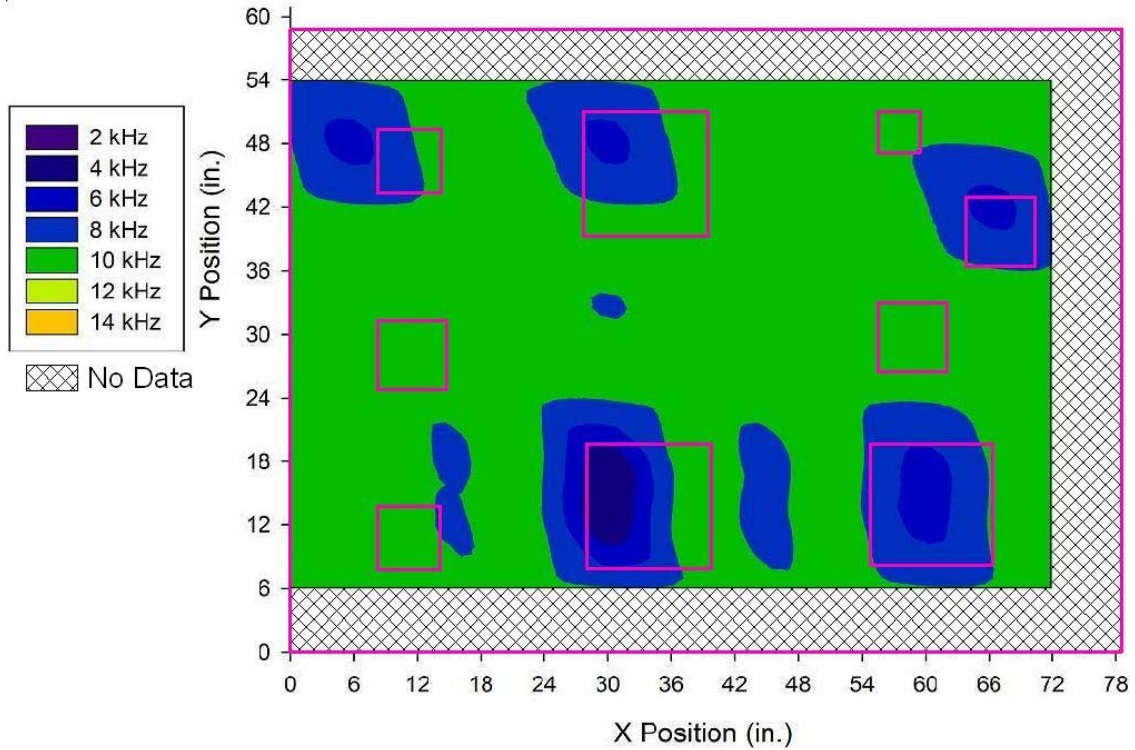


Figure 2.9: Contour plot of defected slab from AIS prototype scan with 5/8" impactor at 6"o.c.

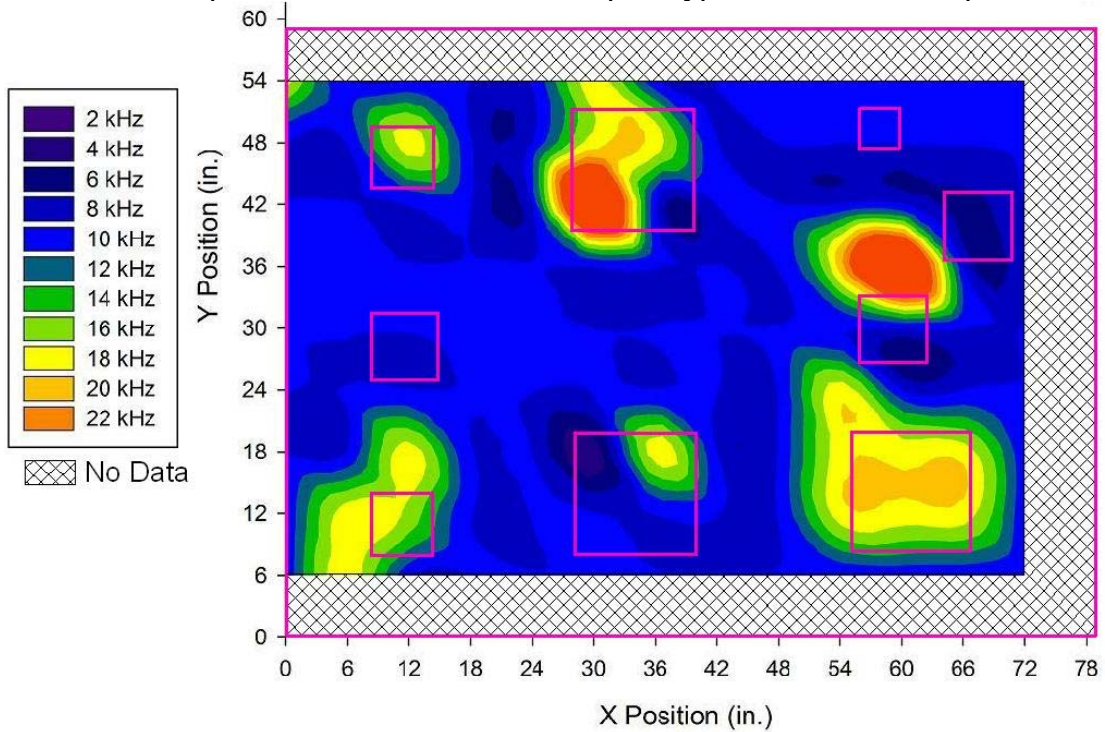


Figure 2.10: Contour plot of defected slab from AIS prototype scan with 5/16" impactor at 6"o.c.

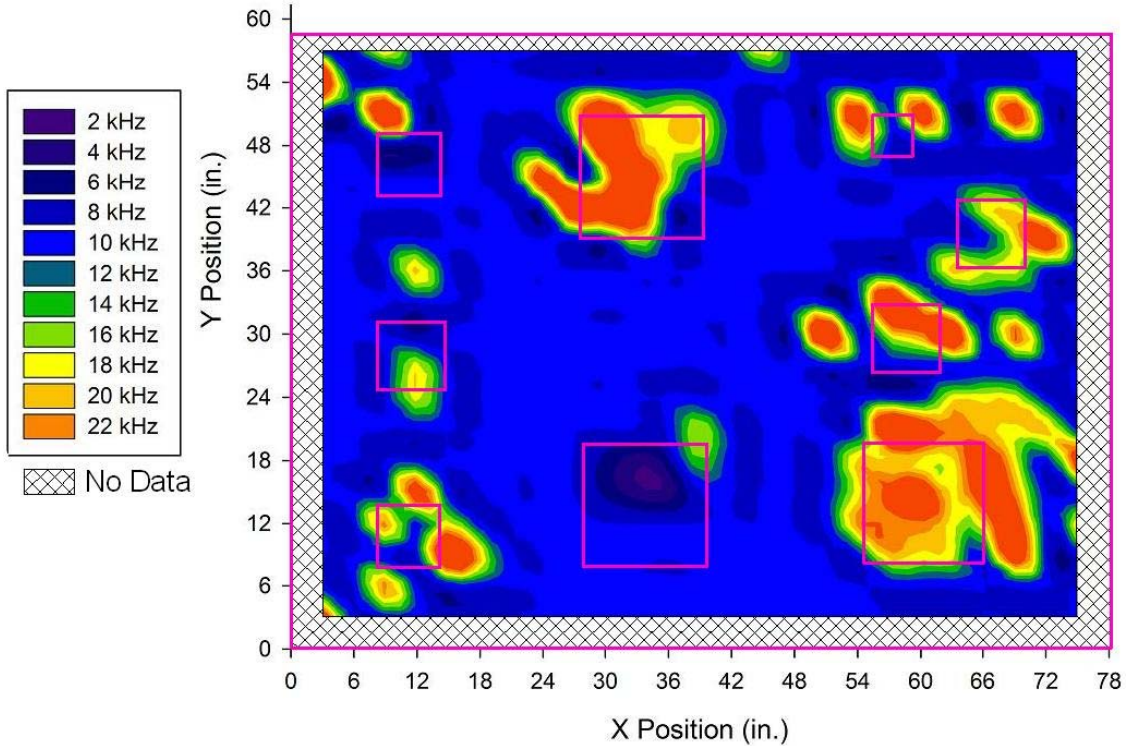


Figure 2.11: Contour plot of defected slab from AIS prototype scan w/ 5/16" impactor at 3" o.c.

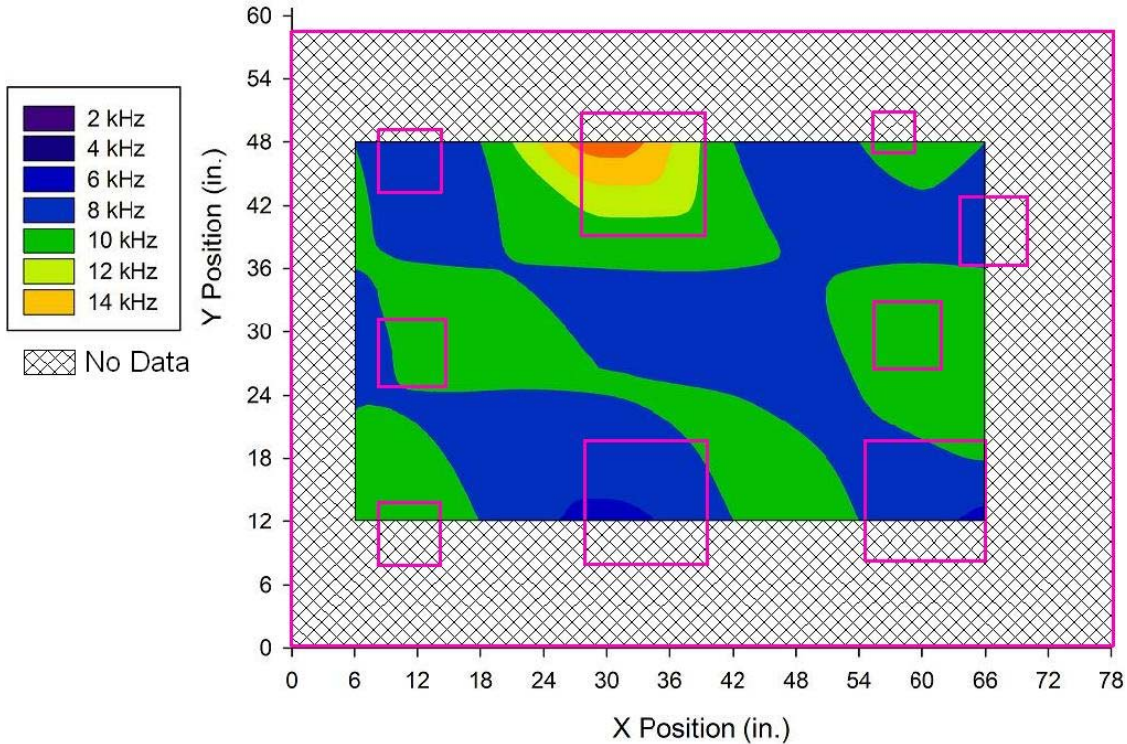


Figure 2.12: Contour plot of defected slab from AIS prototype scan w/ 1/2" impactor at 12" o.c.

The determination of what frequency peak to use at an individual impact location was subjective over the course of work performed. However, a set of guidelines were followed to introduce some degree of objectivity to the choosing of which frequency peak in the response spectrum

would be used. These guidelines were developed from the recommendations given in Chapter 24 of Sansalone and Streett (1997).

Prior to any actual testing being done, information was gathered about the slab to be tested. Given the laboratory setting of the testing, items such as slab thickness, reinforcing and defect locations, and concrete compressive strength were easily obtainable. Knowing these basic parameters, selection of an impactor size to be used could be determined based on Equations 1.1, 3.2, and the following equations developed by Sansalone and Streett (1997):

$$d_{min} = 7D \quad (\text{Eq. 3.1})$$

$$l_{min} = 14D \quad (\text{Eq. 3.2})$$

Where:

$d_{min}$  = minimum depth of flaw that can be detected (m)

$l_{min}$  = minimum lateral size of flaw that can be detected (m)

$D$  = impactor diameter (m)

These equations can be combined to form a reference table relating impactor diameter, contact time, maximum useful frequency, and minimum depth/size of flaw able to be detected, based on an assumed P-wave velocity of 4000m/s (Sansalone and Streett, 1997).

Table 2.4: Approximate relationship of impactor size on key detection limits

<b>Impactor Diameter (in.)</b>	<b>Contact Time (<math>\mu</math>s)</b>	<b>Maximum Useful Frequency (kHz)</b>	<b>Minimum Depth (in.)</b>	<b>Minimum Lateral Size (in.)</b>
1/8	14	91.65	0.875	1.750
3/16	20	61.10	1.312	2.625
	27	45.83	1.750	3.500
1/4				
5/16	34	36.66	2.187	4.375
3/8	41	30.55	2.625	5.250
7/16	48	26.19	3.062	6.125
1/2	55	22.91	3.500	7.000
9/16	61	20.37	3.937	7.875
5/8	68	18.33	4.375	8.750
11/16	75	16.66	4.812	9.625
3/4	82	15.28	5.250	10.500
13/16	89	14.10	5.687	11.375
7/8	96	13.09	6.125	12.250
15/16	102	12.22	6.562	13.125
1	109	11.46	7.000	14.000

Since the slab thickness was known, an assumed P-wave velocity of 4000 m/s could be used for a quick estimation of the response frequency associated with the full slab thickness. P-wave velocity tests were then run to determine a more accurate slab thickness frequency using the measured velocity. Additional frequency peaks for known depths of items such as reinforcing layers were also calculated using the measured P-wave velocity. With the known P-wave velocity and an impactor size selected, the first IE tests were performed on a known or at best suspected undefected portion of the slab to confirm that the calculated slab thickness frequency matched with the tested slab thickness frequency. Upon this confirmation, the slab was fully scanned and data recorded.

After completion of scanning, the frequency spectra from each impact event/point were reviewed and compared to each other in order to determine the validity of the data obtained. Specific items of importance that were looked for in the frequency response spectra were anomalous peaks that were repeated between many different impact locations. Some examples of these anomalous peaks that were found and ignored in the process of peak picking were 1/f peaks/noise, frequency peaks that corresponded to a seemingly random location in the slab, and frequency peaks above the maximum range for that size impactor as given in Table 2.4. Figures 2.13 and 2-14 show some examples of the different spectra from the scan of the defected slab and how they relate to the subjective nature of peaking frequency peaks.

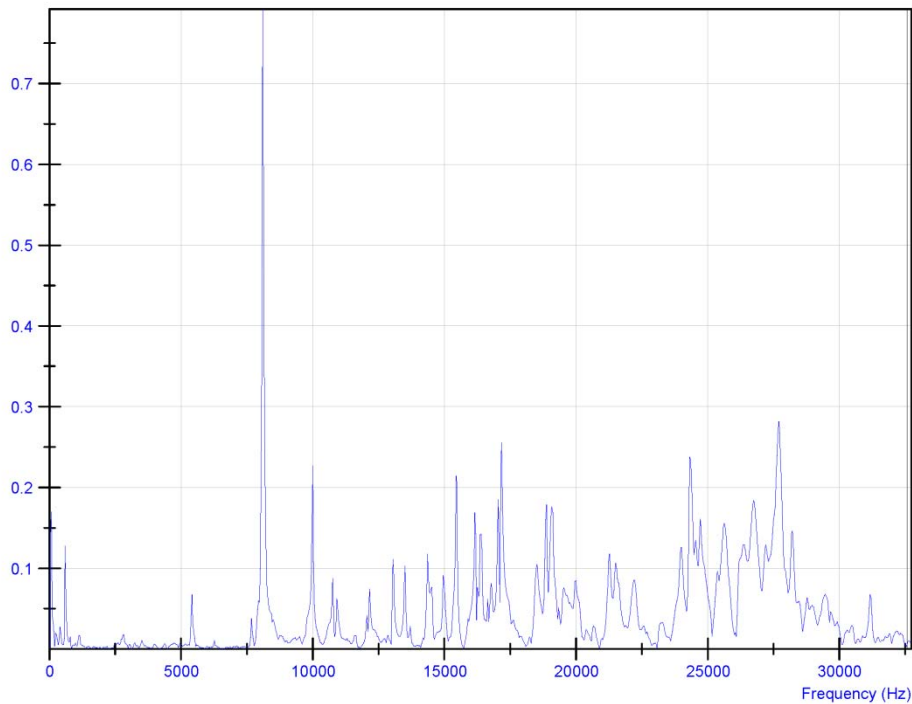


Figure 2.13: Example of a “clean” frequency spectrum from defected slab scan

An ideal scan of a slab would produce nothing but the type of frequency spectra as shown in Figure 2.13. However, the most common of spectra with anomalous frequency peaks was a spectrum with a sharp peak around 24 kHz. Sometimes these peaks were not the highest amplitude and sometimes they were as shown in Figure 2.14.

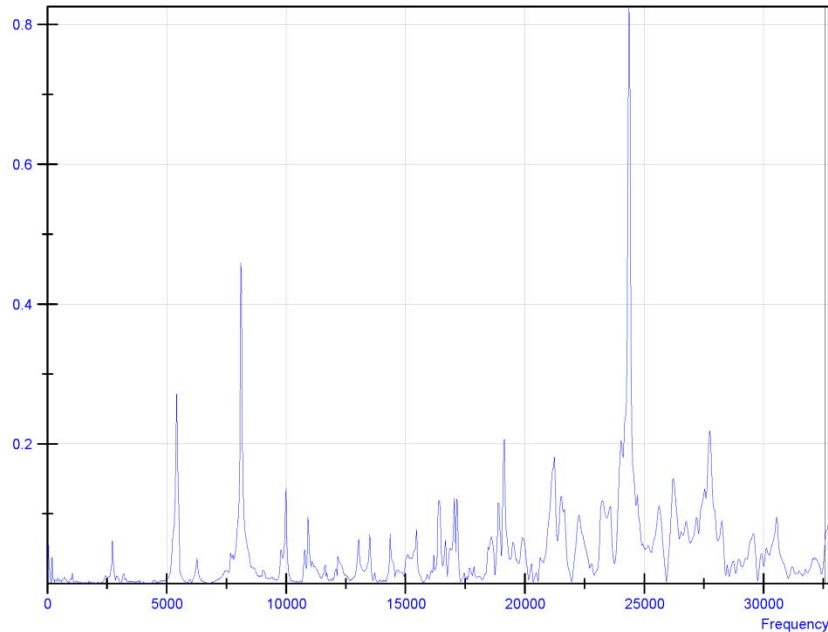


Figure 2.14: Example of a frequency spectrum from defected slab scan with a spike at 24 kHz

While these peaks around 24 kHz were not present in every frequency spectrum, they were present in some form in the sizable majority of them. By Equation 1.1a, a peak at this frequency would correspond to an approximate depth of 3.25” by from the surface of the slab where no layers of reinforcing or defects were intentionally placed. Additionally, the slab could not be forensically analyzed due to its need to be kept intact for future research. These factors led to the ignoring of frequency peaks centered around 24 kHz for the purpose of peak picking for the creation of contour plots.

## 2.2. Field Testing of Concrete Roof Slabs

Field testing was performed on one way reinforced concrete slabs as a means of demonstrating the effectiveness of using the IE method and the AIS prototype for detecting non-visible defects within these slabs. Field testing of the AIS prototype consisted of two categories of testing, *in situ* testing and *ex situ* testing. Initial *in situ* testing was performed in the spring of 2011, with *ex situ* testing occurring in the fall of 2011.

The slabs tested over the course of this work were designed as one way reinforced slabs, and as such, the conclusions drawn from this work apply directly to slabs of similar construction, but can be reasonably assumed to apply to different types of structural elements and this may be proven in future work via testing with this prototype on said elements. These slabs were constructed for the dual purpose use as the ceiling/cover slab for the utility tunnels (colloquially referred to as steam tunnels) that run under PSU’s campus. These particular slabs also functioned as the sidewalk surface for pedestrian traffic above the utility tunnels. As such, they were subjected to freeze/thaw cycles and to salting in the winter months.

Specific sections of slabs to be tested were initially chosen after visual inspection, performed by the author, of both the sidewalk side of the slab as well as the utility tunnel side of the slab. Slab locations from both inspections were coordinated by the use of measurements from stationary, benchmarked points, in this case access and storm water grates cast into a portion of the slab that were repeated at a distance of roughly 100' from each other. The slabs were grouped into 'sections' based upon their visual condition. A total of six sections were identified and chosen for testing. These sections were further divided into slabs of a more manageable size called 'units'. The location of the division of the section into units was based upon control joint locations in the sidewalk side surface. Each unit division resulted in an end slab size of approximately 60"× 84" in size. Table 3.5 presents the breakdown of each section by number of units and observed condition. Specific dimensions for each unit slab are given in Table 3.6

Table 2.5: Classification of concrete slab test sections

<b>Section</b>	<b># of Units</b>	<b>Hypothesized Condition Based on Visual Inspection</b>	<b>Reasoning</b>
1	3	Good	No visible flaws on underside and only 1 small area of surface spalling on sidewalk surface on unit 3.
2	2	Poor	Visible spalling and degradation of rebar on underside. Worn surface but no apparent defects on sidewalk surface.
3	2	Good	No visible flaws on underside, and only slight wearing on sidewalk surface.
4	4	Poor	Visible spalling and degradation of rebar on underside. Large defect on surface between unit 1 and 2, and additional surface spalling on units 2, 3, and 4.
5	3	Questionable	Visible repair patches on underside, and slight spalling on sidewalk surface of unit 1.
6	3	Questionable	Visible minor early stage spalling on underside. Spalling on sidewalk surface on unit 1, and surface crack at sound end of Section 3.

Table 2.6 Physical dimensions of Units

Section	Unit	Length (in.)	Width (in.)	Thickness (in.)	Reinforcing Type (per Fig. 6-2)
1	1	61	84	6.5	Double Mat
1	2	61	84	6.3	Double Mat
1	3	61	84	5.7	Double Mat
2	1	-	-	-	-
2	2	-	-	-	-
3	1	66	84	6.0	Single Mat
3	2	65	84	5.9	Single Mat
4	1	62	84	6.2	Single Mat
4	2	62	84	5.6	Single Mat
4	3	62	84	5.7	Single Mat
4	4	62	84	6.2	Single Mat
5	1	59	83	6.2	Single Mat
5	2	60	83	6.4	Single Mat
5	3	60	83	6.5	Single Mat
6	1	60	84	6.2	Single Mat
6	2	61	84	6.1	Single Mat
6	3	60	84	6.2	Single Mat

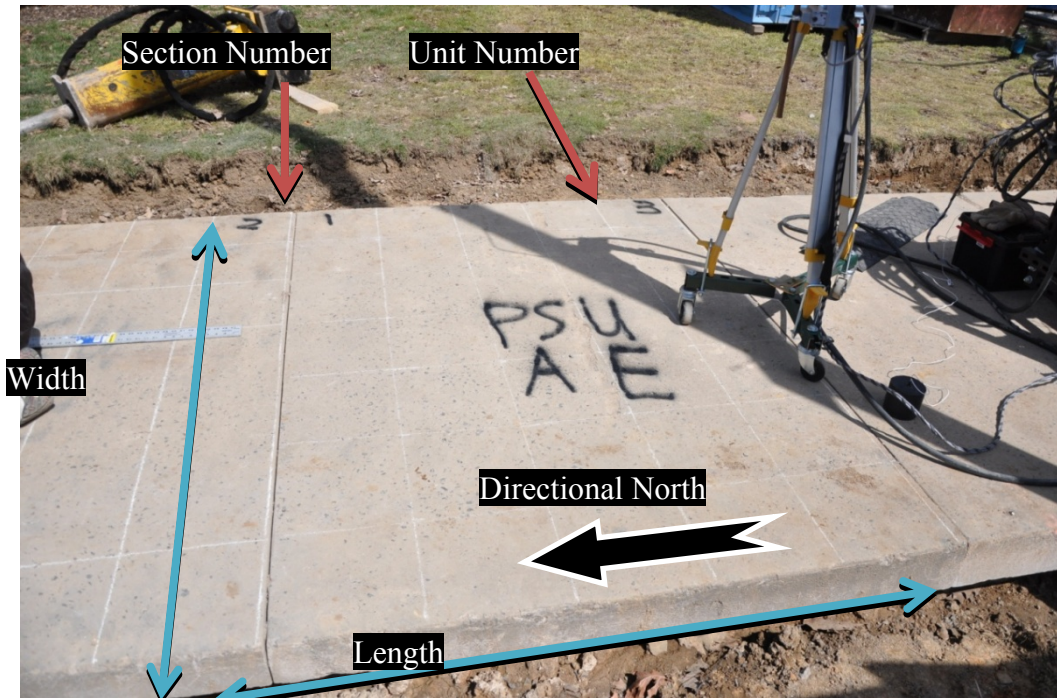


Figure 2.15 Layout of Section/Units

Reinforcing layouts in one direction were observed based upon visual inspection of the various slabs after removal from the Shortlidge Road location. Two different reinforcing layouts were used in the slabs. The first and more typical layout consisted of a single mat of #3 bars at 7"-

9"o.c. located at the bottom of the slab. The second reinforcing layout was a double mat of #3 bars at 8"-9"o.c. located at the top and bottom of the slab with approximately 2" between the layers. In both cases, bottom cover was approximately 1.5"-2".

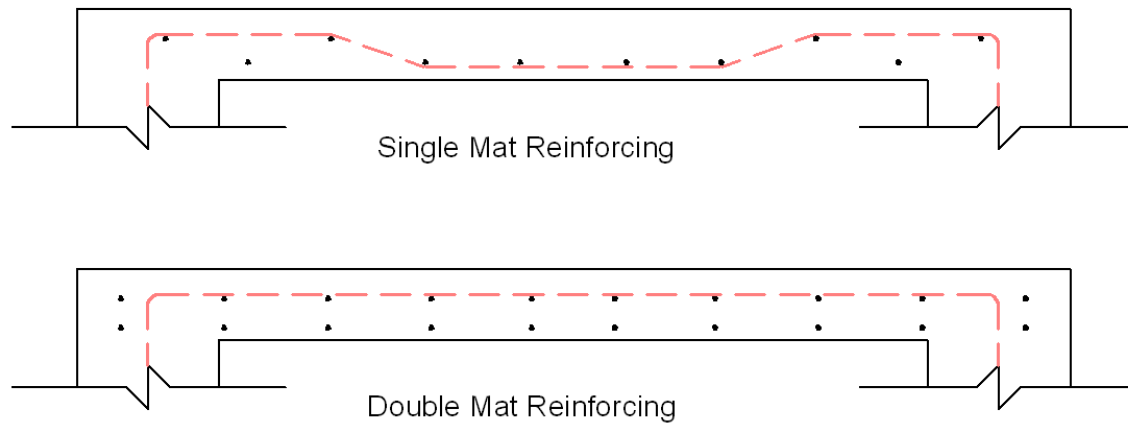


Figure 2.16: Single mat reinforcing and double mat reinforcing slab cross sections

Reinforcing layouts in the orthogonal direction of the saw cuts could not be fully determined at that point since construction documents for the slabs were not able to be obtained. However transverse reinforcing bars were observed at a limited number of saw cuts and bar placement for the two different layouts was recorded. Concrete strength of the slabs was also unknown at the time of testing due to the lack of construction documents.

All of the slabs outlined in the Table were tested according to the procedure given below. Two representative tests will be described in detail. For details of the results of the other slabs tested, the reader is referred to Riewestahl (2011)

**2.2.1 In Situ Testing.** *In situ* testing was performed starting in March of 2011 and concluded at the end of April 2011 due to removal of the slabs. The availability and testing of the sections/units was coordinated with GMM and performed as scheduling and weather permitted. Impactor diameter, impact unit spacing, and system air pressure were varied throughout the course of *in situ* testing. The sampling rate and number of samples were fixed at 51.2 kHz and 2000 respectively. This resulted in a frequency resolution of 25.6 Hz. P-wave velocity measurements were not performed *in situ* because that portion of the testing software was not completed at the time of testing. A summary of the *in situ* testing performed is given in Table 2.7.

Table 2.7: Summary of *in situ* testing performed

Section	Unit	Grid spacing (in. o.c.)	Impactor Diameter (in.)	System Air Pressure (psi)	Contour Plot Figure Number
1	2	12	7/16	20	--
1	3	12	5/8	20	3.17
2	1	12	5/8	20	3.18
2	1	12	3/8	10	--
2	1	12	7/16	10	--
2	1	6	3/8	10	--
2	2	12	5/8	20	--
3	1	6	7/16	20	--
3	2	12	7/16	20	--
3	2	12	5/8	20	--
4	1	12	7/16	20	--
4	2	8	7/16	10	--
5	1	12	3/8	20	--

Data from the *in situ* testing was compiled into contour plots for each unit.

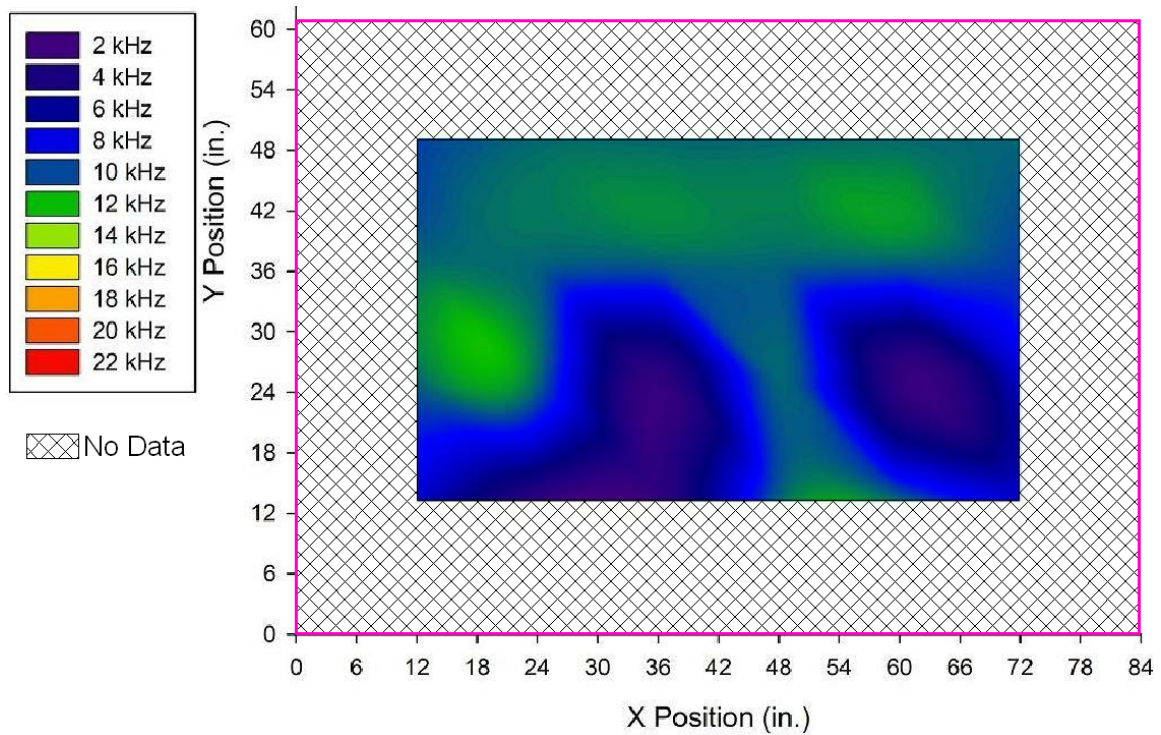


Figure 2.17: *In situ* data contour plot of Section 1 Unit 3 with 5/8" impactor at 12" o.c.

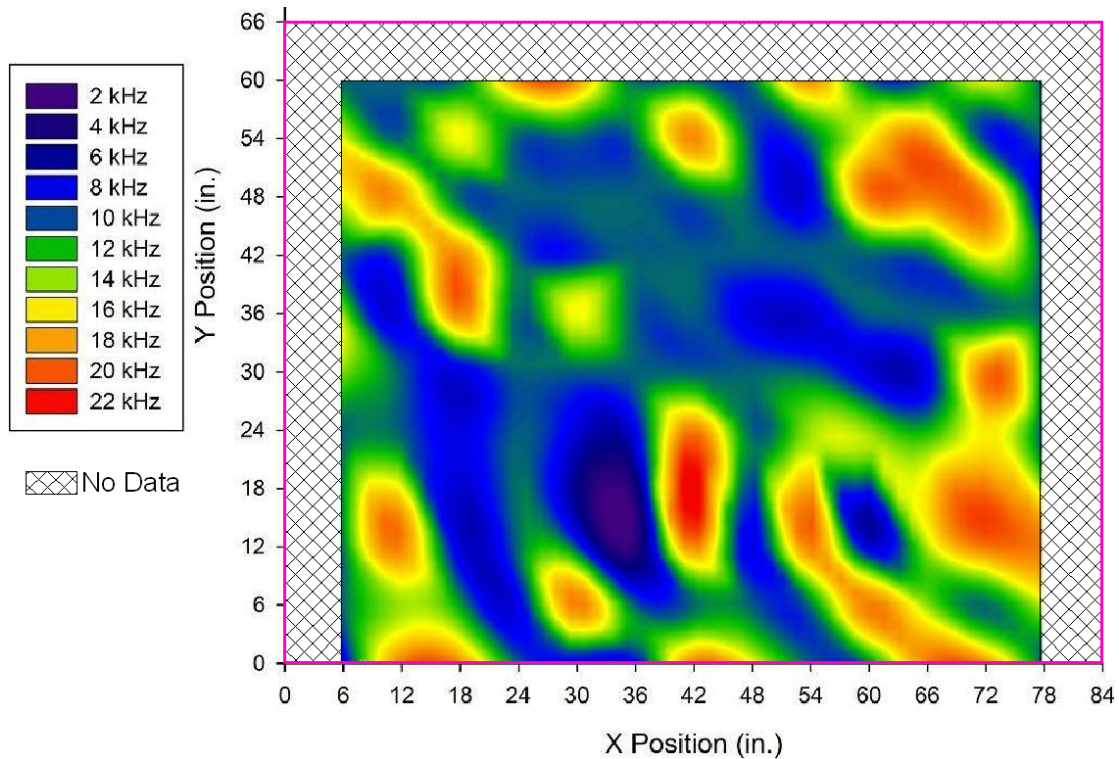


Figure 2.18. *In situ* data contour plot of Section 3 Unit 1 with 7/16" impactor at 6" o.c.

**2.2.2 Ex Situ Testing** Upon removal of the various slabs from their original location, the slabs were transported to off-site storage. Prior to removal, slabs were labeled with spray painted markings with the *in situ* section and unit numbers to allow for referencing of slab data between *in situ* and *ex situ* testing. The slab's *in situ* orientation with respect to directional north was also noted and labeled on the slabs. The slabs were supported by wood pallets placed at the edges of the slab, shown in Figure 3.19, in order to approximate the *in situ* support condition.



Figure 2.19: Slab off-site storage support condition

Table 2.8: Summary of *ex situ* testing performed

Section	Unit	Grid spacing (in. o.c.)	Impactor Diameter (in.)	Sampling Rate (Hz)	Number of Samples	Freq. Resolution (Hz)	Contour Plot Figure Number
1	2	6	3/8	76800	1536	50	--
1	3	6	3/8	76800	1536	50	3.20
3	1	6	3/8	102400	1000	102.4	3.21
3	2	6	3/8	51200	1000	51.2	--
4	1	6	3/8	76800	1024	75	--
4	3	6	1/2	51200	1024	50	--
5	1	6	3/8	76800	768	100	--
5	2	6	3/8	76800	1536	50	--
6	1	6	1/2	51200	512	100	--
6	3	6	1/4	102400	2048	50	--

Data from the *ex situ* testing was compiled into contour plots for each unit in the same manner previously performed for both the laboratory and *in situ* testing.

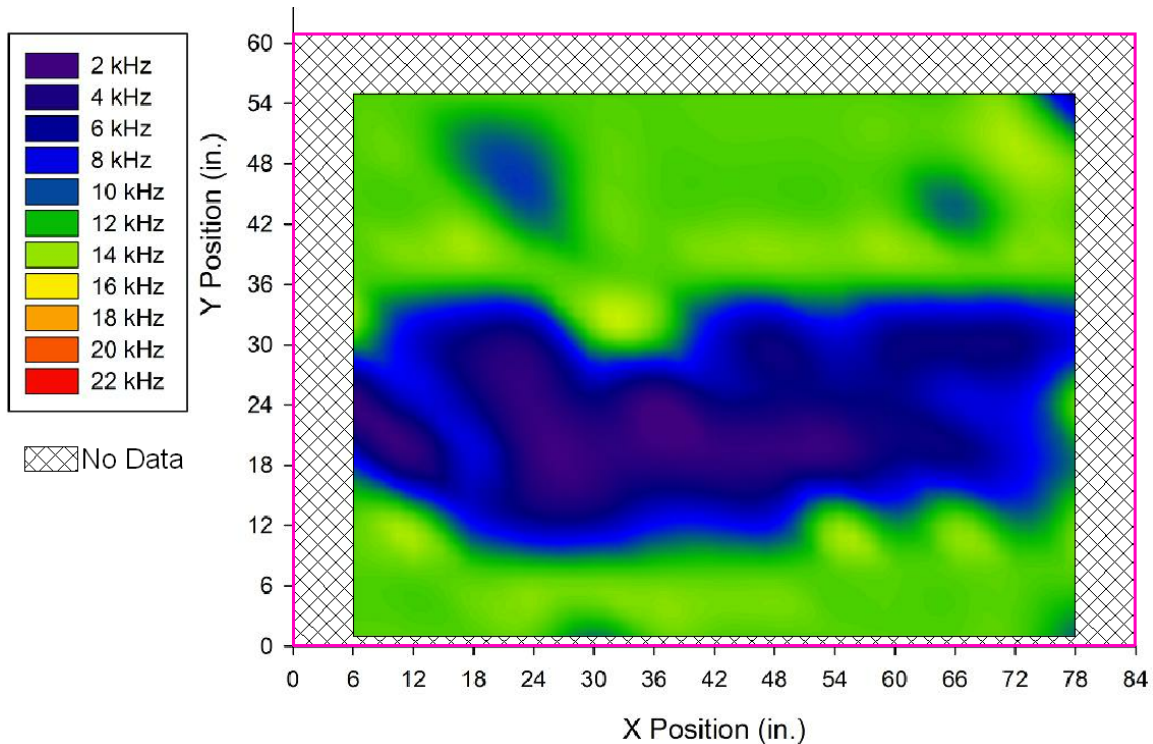


Figure 2.20: *Ex situ* data contour plot of Section 1 Unit 3 with 3/8" impactor at 6" o.c.

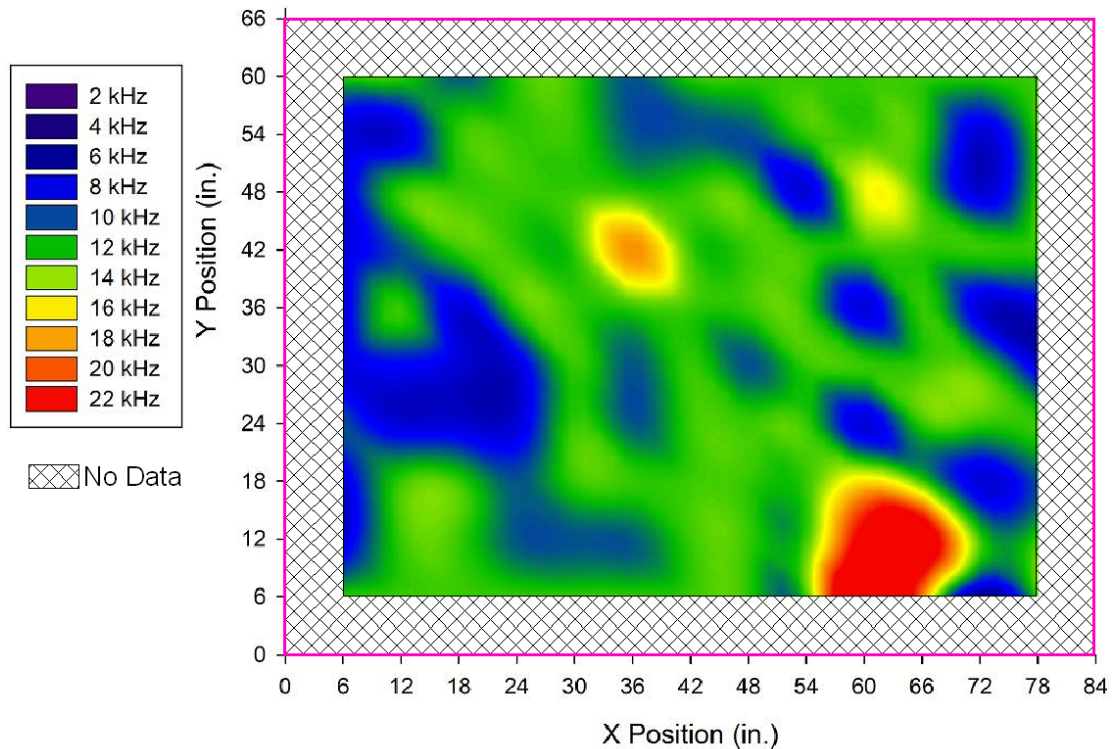


Figure 2.21: *Ex situ* data contour plot of Section 3 Unit 1 with 3/8” impactor at 6”o.c.

### 2.3. Forensic Analysis of Concrete Roof Slabs

For proper validation of the AIS prototype as an effective tool for locating flaws in concrete slab, destructive evaluation techniques were performed on a group of seven slabs in order to either confirm or deny the findings from the *in situ* and *ex situ* testing of the slabs. The selected slabs to be forensically analysis were; Section 1 Unit 2, Section 1 Unit 3, Section 3 Unit 1, Section 3 Unit 2, Section 4 Unit 1, Section 5 Unit 1, and Section 6 Unit 3. These particular slabs were chosen to be analyzed since they covered a representative sample of slab conditions of “good”, “poor”, and “questionable” based initial visual inspection previously performed and highlighted in Table 6-1, as well as presenting some interesting features in the *in* and *ex situ* contour plot for each individual unit. To gain access to specific locations of interest in the slabs, the slabs were cut with a concrete saw, and the findings from these locations were compared with the findings of previously assembled IE scan data contour plots.

**2.3.1 Analysis Approach:** Using the previously assembled contour plots based on *in situ* and *ex situ* testing data for the individual units within each section as a starting point, locations of interest such as areas suspected flaws and suspected undefected areas were selected for destructive forensic analysis. By examining these locations of suspected sound and defected portions of the concrete slabs, conclusions as to the ability of the AIS prototype to accurately detect flaws could start to be made. From the contour plots, the area of the slabs shaded in green are areas thought to contain no defects, while areas that show up as either blue or red are hypothesized to contain a defect. Blue/Purple areas are made up by a dominant frequency peak

in the frequency spectrum from the measured location that is below the expected thickness frequency of the slab based on field measurements and testing, and by Equation 1.6a. A possible cause of this type of response includes excitation of the flexural mode of vibration of the slab instead of the plate thickness mode due to a possible delamination. Another possible cause for a lower frequency response is the stress wave having to travel through material that is more “acoustically soft” and as a result the P-wave travels at a lower velocity. Red/Yellow areas are impact locations that exhibited a dominant frequency peak that is above the expected thickness frequency. A possible cause for this includes a delamination within the concrete that is still excited in the plate thickness mode, but due to the apparent reduced thickness of concrete caused by the delamination returns a signal higher than the expected slab thickness frequency. Another possible cause is an increased P-wave velocity due to material inhomogeneity in that the P-wave travels faster through that location than in other locations in the surrounding slab.

The selected locations were then exposed for analysis by saw cutting of the concrete slab. Saw cutting of the slabs was determined to provide the best means of access to the desired locations in terms of expedience and minimizing damage from gaining that access to the surrounding areas of the slabs. The saw cutting was performed by PSU OPP using a walk behind concrete saw. During saw cutting, the slab was supported on opposing sides of the cut location with CMU blocking and shims to prevent the slab from falling in on itself and potentially causing additional damage to the slab.



Figure 2.22: Saw cutting of slabs *ex situ*

**2.3.2 Slab Cut Locations:** A total of 15 cuts were made in the seven slabs previously mentioned. Every resulting portion of slab was labeled prior to cutting according to the Section and Unit number and then given an additional letter designation for each portion of the slab that would exist after being saw cut. The portion of the slab that was the furthest left was designated as sub-unit A, the next piece as sub-unit B, and so on till all the sub-units were labeled. This was done as a means to organize the resulting sub-units so that the slabs could be placed in the correct order after the cutting process if they were moved.

After cutting, the slab sub-units were spread apart for inspection by the use of a forklift. The sub-units were placed on blocks in a similar fashion as was done during saw cutting to facilitate being able to move the sub-units easily with the forklift.

Section 1 Unit 3 was selected for a singular apparent defected band running along the slab at approximately mid span of the slab. Only a single cut location was selected, as indicated in Figure 3.23, due to the fairly uniform distribution of slab area with hypothesized defects.

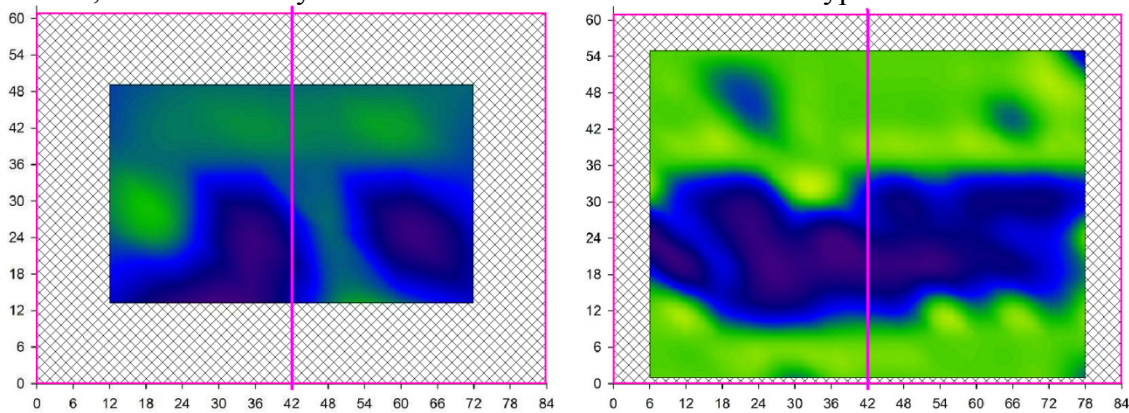


Figure 2.23: Saw cut locations on Section 1 Unit 3 (Left: *in situ* contour plot. Right: *ex situ* contour plot)

Section 3 Unit 1 was selected for the three cut locations shown in Figure 3.24 due to the seeming incongruity of the slab's condition between the *in situ* and *ex situ* contour plots. Given the grid spacing used (6" o.c. in each case) and the close nature of impactor diameter (7/16" for the *in situ* test and 3/8" for the *ex situ* test) it would be assumed that the contour plots from each test would have been more similar.

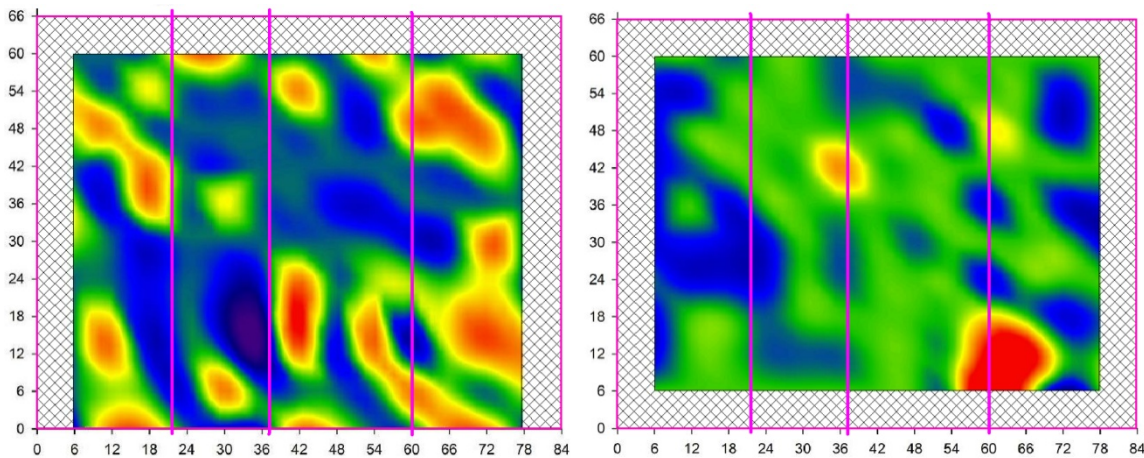


Figure 2.24: Saw cut locations on Section 3 Unit 1 (Left: *in situ* contour plot. Right: *ex situ* contour plot)

**2.3.3 Results.** After saw cutting on all selected slabs was completed, the resulting sub-units were spread apart and wiped down with a moist rag to remove dirt and debris from the cross section leftover from the saw cutting. After this was complete slabs were inspected and photographed. Inspection was carried out visually, both by the naked eye and with the use of a 50 power magnifying glass. In addition to the visual inspection, sections were also gently tapped with a hammer to dislodge any loose pieces of concrete. If defected areas were found during inspection they were marked by permanent marker. Cracks and delaminations were marked by underlining and areas of voids or honeycombing were marked by circles around them.

During the forensic analysis of Section 1 Unit 3 the same features were examined in detail as in the analysis of Section 1 Unit 2, mainly the determination of whether a defect existed in the middle band of the slab as suggested by the contour plots from field testing. Visual inspection revealed a large horizontal crack within the slab at the mid span area as shown in Figure 7-13 and Figure 2.25 spanning from roughly 13” to 31” within the slab.



Figure 2.25: Cross section of Section 1 Unit 3 sub-unit A

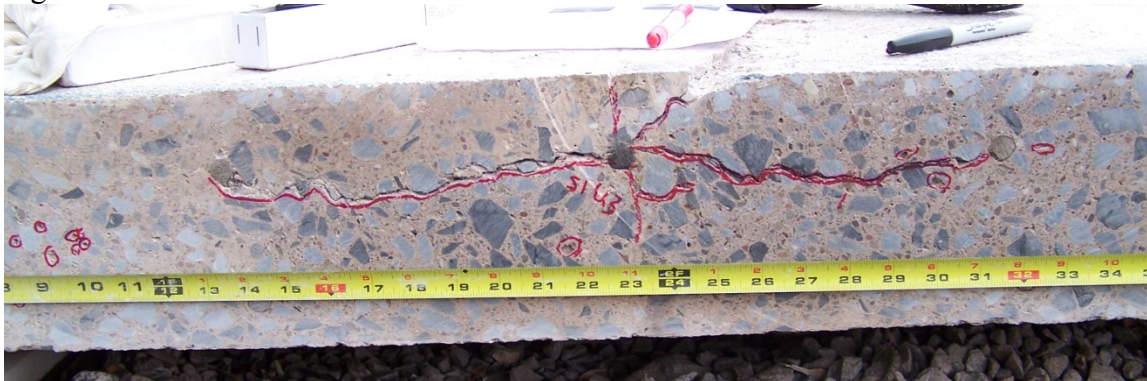


Figure 2.26: Close up of cross section of Section 1 Unit 3 sub-unit A

The inspection of Section 3 Unit 1 cross sections revealed an odd assortment of things. The first oddity noticed was the appearance of small section of noticeably different concrete material. These areas measured roughly only 2” long and around 4” high, and appeared towards the end of the slab. Shown in Figure 3.27, these areas have noticeably no large aggregate like the surrounding areas and also appear to have a distinct horizontal separation within them about

halfway up. Given their height, small nature, and locations, it is probable that these areas are actually the chairs that the slab's reinforcing was placed on during construction of the slab.



Figure 2.27: Close up of differing concretes in cross section of Section 3 Unit 1 sub-unit C

No apparent defects were found in the cross section between sub-units A and B other than the aforementioned small change in concrete material located between 26" and 28". The cross section between sub-units B and C exposed a 1"×2" LLH tubular metal insert running from 3" to 5" and some small areas of unconsolidated concrete from 35" to 45" as shown in Figure 3.28.



Figure 2.28: Cross section of Section 3 Unit 1 sub-unit C between B and C

The last cross section of this unit between sub-units C and D shown in Figure 3.29, again revealed presumed reinforcement chairs at 6" and at 56" accompanied by areas of unconsolidated concrete at 22", 31" and from 47" to 57".



Figure 2.29: Cross section of Section 3 Unit 1 sub-unit C between C and D

### 3. Experimental Work on Masonry Walls: Description and Results

#### 3.1 Masonry Wall Specimens: Lab

The air-coupled impact-echo method was applied to the three 64" by 64", triple-wythe solid brick wall specimens. The wall specimens all have: common bond with full brick header every 6 courses, unreinforced. In general, every stretcher in alternate courses was tested. Wall Specimens A.1, A.2, B.1, and B.2 each have thirty-two (32) test points across the wall specimen. Wall Specimen C.1, C.2, C.3, and C.4 each have sixteen (16) test points. These walls were constructed in the warehouse of Masonry Preservation Services. The air-coupled impact-echo method was applied to the walls on three test dates: April 15, May 10, and September 23, 2011.

Wall Specimen A.1 was built with an intentional bond disruption to imitate poor bonding. The mortar was allowed to partially set for a few hours and then manually shifted to disrupt mortar to brick bond. Wall Specimen A.2 has partially filled joints to replicate joints with poor bonding. The partially fill head, bed, and collar joints simulate poor workmanship. Wall Specimen B.1 has cored brick in lieu of the solid brick to be able to note the difference between a cored within the brick versus a bond disruption. Wall Specimen B.2 has unfilled collar joints to poor bonding between collar joints. Wall Specimen C.1 has a steel beam embedded within the brick. Wall Specimen C.2 has a historic terra cotta panel mounted to the brick. Wall Specimen C.3 contains normally laid solid brick with a header course. Wall Specimen C.4 has a 0.25 inch thick layer of stucco over the brick.



Figure 3.1: Wall Specimen A1, A2



Figure 3.2: Wall A.1 – Bond Disruption



Figure 3.3: Wall A.2 –Partially Filled Joints



Figure 3.4: Wall Specimen B1, B2



Figure 3.5: Wall B.1 – Cored Brick



Figure 3.6: Wall B.2 –Unfilled Collar Joints



Figure 3.7: Wall Specimen C.1, C.2, C.3, C.4



Figure 3.8: Wall Specimen C.1 – Steel Beam and Wall Specimen C.2 – Terra Cotta Panel

**3.1.1 Testing:** The Impact-Echo (IE) assessment method was conducted to investigate the characteristics and the conditions of selective locations in the masonry. For an intact, homogeneous material, the fundamental equation of impact-echo analysis is equation 3.1,

$$f = \frac{\beta C_p}{2T} \quad (\text{Eq. 3.1})$$

where  $C_p$  is the propagation velocity of the p-waves,  $t$  is the thickness of the material,  $f$  is the fundamental frequency (usually called the thickness frequency) and  $\beta$  is a modification factor for the shape of the specimen. Transverse echoes in a beam require modification by a  $\beta < 1.0$ . The  $\beta$  factor for a plate like structure (depth  $\ll$  width) is 0.96.

The P-wave speed was calculated using the control wall, Wall Specimen C.3. The average thickness frequency, as determined by testing, for Wall Specimen C.3 was 6.7 kHz. Using the values in Table 3.1 into equation 3.1, the thickness frequency was verified to be 6.7 kHz. For the triple-wythe solid brick wall, the brick p-wave speed was 4450 m/s and the mortar p-wave speed was 3250 m/s.

Table 3.1: Thickness frequency variables for triple-wythe wall.

	$\beta$	$C_p$	T
Brick Layer 1	0.96	4450 m/s	0.092 m
Mortar	0.96	3250 m/s	0.015 m
Brick Layer 2	0.96	3250 m/s	0.092 m
Mortar	0.96	4450 m/s	0.015 m
Brick Layer 3	0.96	3250 m/s	0.092 m

**3.1.2 Results:** The results of the air-coupled impact echo testing indicate areas of bonding and imperfect bond. Bonding is reduced due to the presence of voids, defects, discontinuities and honeycombing. The spectrum data was plotted, and then using standards from Sadri (2003) the bonding type was determined for each response in Figure 3.9.

Wall Specimen A1 tests results indicated poor bonding and very poor bonding at many locations. Wall Specimen A2 test result indicated poor bonding: voids. Wall Specimen B1 showed very good bonding, while Wall Specimen B2 indicated poor bonding voids. Then Wall Specimen C1 had very good bonding. Wall Specimen C2 had very good bonding. Wall Specimen C3 had very good bonding as well. Finally, Wall Specimen C4 had very good bonding.

The application of this system shows some ability to detect disruptions in the bond between wythes, although a general disruption, such as the disrupted mortar joints appears to be easier to detect than intermittent voids. The use of cored bricks did not materially affect the quality of the results of this survey.

### 3.1.3 Bonding Classification

Bonding Type		A. Sadri, NDT&E Int'l 36 (2003)	Beverly Minster Field Test
VGB	<p><b>Very Good Bonding</b></p> <p>Very good bonding (VGB) indicates that the maximum peak frequency is generated and dominates the other minor reflections.</p>	<p>Fig. 6. Frequency spectrum from N15, very good bonding.</p>	
PBH	<p><b>Poor Bonding Honeycombing</b></p> <p>When the frequency spectra multiple peak frequencies appear at a close range between the thickness frequency and the brick/grout interface frequency, the bonding is classified as poor bonding honeycombing (PBH).</p>	<p>Fig. 6. Frequency spectrum from M5, poor bonding and presence of honeycombing.</p>	
PBV	<p><b>Poor Bonding Voids</b></p> <p>A series of high amplitude peaks in the frequency spectra between reflections from the thickness frequency and the brick/grout interface frequency is identified as fair bonding voids (FBV).</p>	<p>Fig. 7. Frequency spectrum from M13, fair bonding, but presence of voids within the core.</p>	
VPB	<p><b>Very Poor Bonding</b></p> <p>When the reflection frequencies are at lower values than the thickness frequency, the masonry is identified as having very poor bonding (VPB).</p>	<p>Fig. 5. Frequency spectrum from S87, very poor bonding.</p>	
WS	<p><b>Weak Signal</b></p> <p>If the frequency amplitude for the full thickness is smaller than the defect peak frequency, it indicates that not much energy has passed through the structure and most of the impact energy is reflected from the anomaly, which is indicated by weak signal (WS).</p>	<p>None</p>	

Figure 3.9. Bonding Classification from Sadri (2003)

- Very Good Bonding (VGB)
- Poor Bonding Voids (PBV)
- Poor Bonding Honeycombing (PBH)
- Very Poor Bonding (VPB)
- Weak Signal (WS)



Figure 3.10: Wall Specimen A.1-Bond Disruption\_Test 1 Results



Figure 3.11: Wall Specimen A.1 Bond Disruption\_Test 2 Results

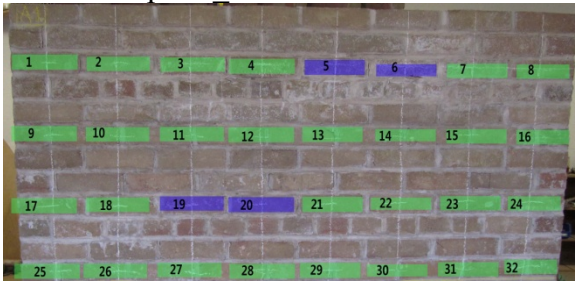


Figure 3.12: Wall Specimen A.1 Bond Disruption\_Test 3 Results



Figure 3.13: Wall Specimen A.2 Partially Filled Joints\_Test 1 Results



Figure 3.14: Wall Specimen A.2 Partially Filled Joints\_Test 2 Results



Figure 3.15: Wall Specimen A.2 Partially Filled Joints\_Test 3 Results



Figure 3.16: Wall Specimen B.1 Cored Brick\_Test 1 Results

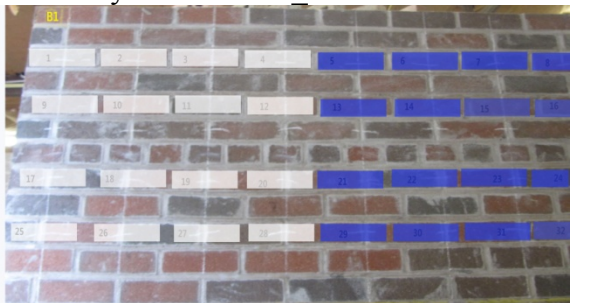


Figure 3.17: Wall Specimen B.1 Cored Brick\_Test 2 Results

- Very Good Bonding (VGB)
- Poor Bonding Voids (PBV)
- Poor Bonding Honeycombing (PBH)
- Very Poor Bonding (VPB)
- Weak Signal (WS)



Figure 3.18: Wall Specimen B.1  
Cored Brick\_Test 3 Results

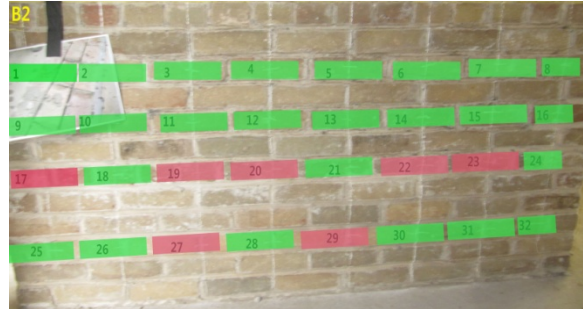


Figure 3.19: Wall Specimen B.2  
Unfilled Collar Joints\_Test 1 Results



Figure 3.20: Wall Specimen B.2\_Test 2 Result  
Unfilled Collar Joints\_Test 2 Results



Figure 3.21: Wall Specimen B.2  
Unfilled Collar Joints\_Test 3 Results

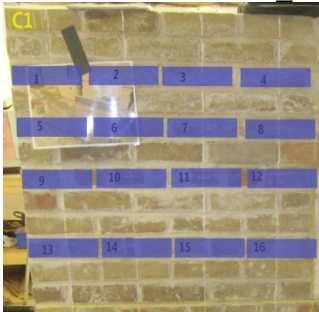


Figure 3.22: Wall Specimen C.1  
Steel Beam\_Test 1 Results

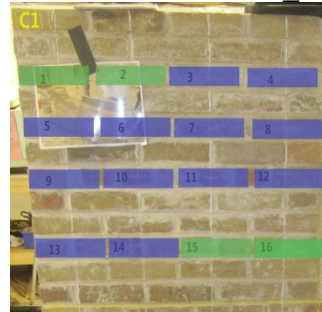


Figure 3.23: Wall Specimen C.1  
Steel Beam\_Test 2 Results



Figure 3.24: Wall Specimen C.1  
Steel Beam\_Test 3 Results

- Very Good Bonding (VGB)
- Poor Bonding Voids (PBV)
- Poor Bonding Honeycombing (PBH)
- Very Poor Bonding (VPB)
- Weak Signal (WS)

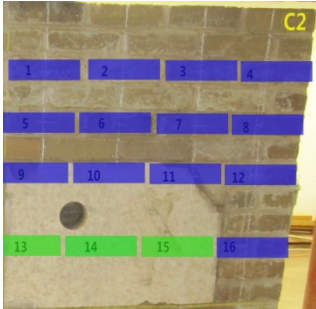


Figure 3.25: Wall Specimen C.2  
Terra Cotta Panel Test 1 Results



Figure 3.26: Wall Specimen C.2  
Terra Cotta Panel Test 2 Results



Figure 3.27: Wall Specimen C.3  
Control Test 1 Results

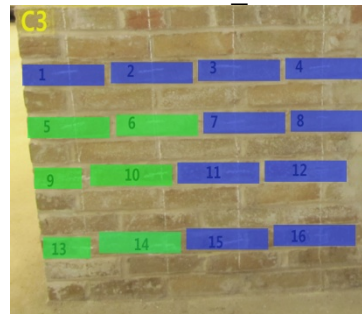


Figure 3.28: Wall Specimen C.3  
Control Test 2 Results



Figure 3.29: Wall Specimen C.3  
Control Test 3 Results



Figure 3.30: Wall Specimen C.4  
Stucco Test 1 Results

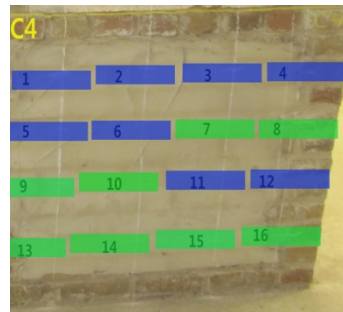


Figure 3.31: Wall Specimen C.4  
Stucco Test 2 Results

## **3.2 Field Tests of Masonry Walls**

The air coupled impact echo system has been used on a variety of field tests. These include: Beverley Minster, Wyoming Seminary, St. Johns, and the Geisinger Medical Center. A large testing program was undertaken in the vaults of Beverley Minster, a 12-14 century church in England. A further testing program was undertaken in the very early stages of this project on the walls of Wyoming Seminary, a three-story load bearing brick masonry building constructed in the mid-nineteenth century. The results of the test on Geisinger Medical Center will be reported here.

### ***3.2.1 Field Test: Geisinger Medical Center***

The air coupled impact echo method was applied to the single wythe masonry façade on the Geisinger Medical Center. The following information about the Geisinger Medical Center Restoration Project was taken from the Masonry Preservation Services Report (2010).

The Geisinger Medical Center is located in Danville, Pennsylvania. This large medical complex, which opened in 1915, is the nation's largest rural health care facility, a tertiary and quaternary medical center recently named one of the top 100 hospitals in the United States. The Abigail Pavilion, designated on original design specifications and drawings by Ewing Cole Rizzio Cherry Parsky Architects – Engineers – Planners as the “Geisinger Medical Center Phase Two Expansion”, was designed circa 1979. The suites were constructed using a structural steel frame with cast-in-place/composite metal deck floor and roof slabs, clad with a wall system comprised of steel studs, interior and exterior sheathing, drainage cavity and 4” face brick. The structure's parapets utilized 6” CMU back-up, precast stone coping and were also faced with the continuous 4” face brick.

The final design at the Abigail Pavilion was a cavity wall with brick veneer over steel stud panel walls. This construction detailing was first adopted during the early 1970's in an effort to reduce costs resulting in lighter less redundant building envelopes. Over the last forty plus years, the Brick Industry Association (BIA), formerly known as the Brick Institute of America, has published and revised standards pertaining to the detailing and construction of masonry walls supported by steel studs. Over time, significant changes were necessitated by problems encountered including: cracking, corrosion of steel relief angles, corrosion of steel stud back-up components, liquid water infiltration (leakage) and the formation of condensation (convergence) occurring within the wall assembly during cold weather conditions.

Since the design of the Abigail Pavilion in 1979, three major changes in recommendations pertaining to brick veneer/steel stud wall detailing and standards have been published by the Brick Industry as Technical Notes 28B, revised February 1980, February 1987, and December 2005.

The recommended changes impacting the Abigail Pavilion's wall detailing, the primary changes/improvements pertain to: 1) the stiffening of steel stud back-up; 2) the use of more robust flashing materials and their extension to daylight; 3) the inclusion of moisture barrier/weather resistant barrier over exterior sheathing as added protection against liquid

moisture entry; 4) the strategic placement of a vapor barrier within the wall assembly; and 5) strong language to encourage consideration of hot dip galvanizing to protect lintels and shelf angles from corrosion.

### 3.2.1.1 Testing:

On May 10, 2011, a field test of the air-coupled impact-echo system was conducted on the Abigail Pavilion at the Geisinger Medical Center.



Figure 3.32: Test Location.



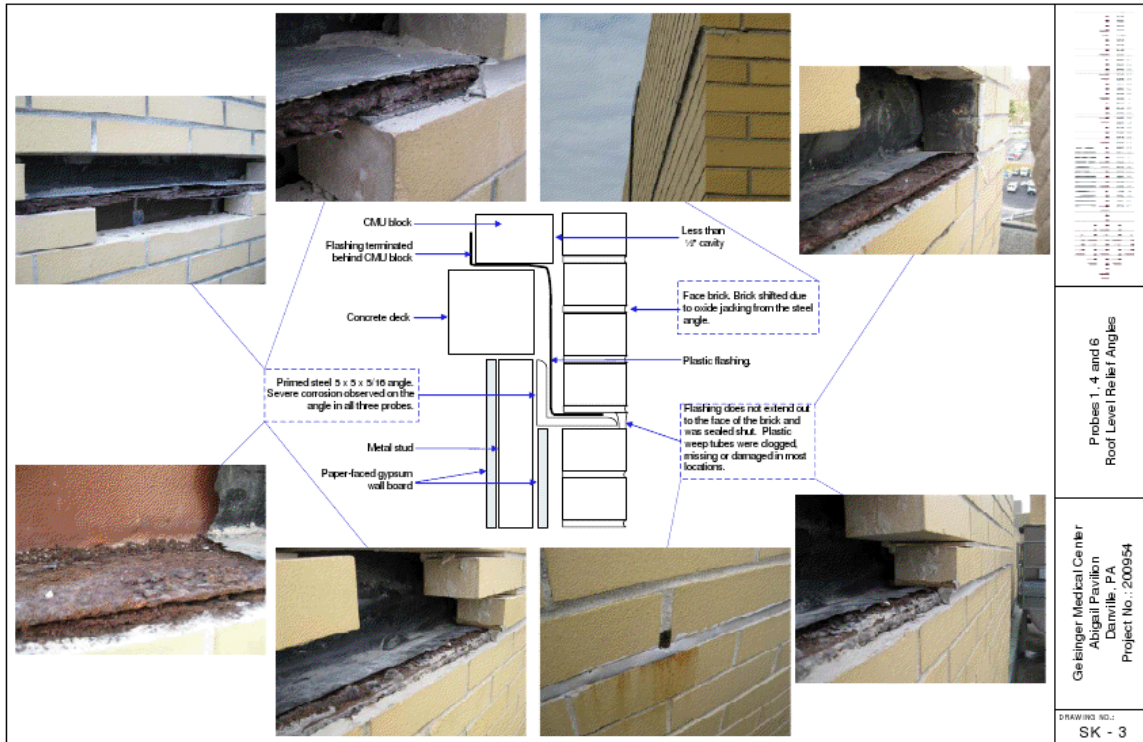
Figure 3.33: Removed brick at test site.



Figure 3.34: Wall tested: a) Lateral view.



b) Wall Section.



a.

Appendix A - Photographs  
Geisinger Medical Center Abigail Pavilion  
Masonry Façade Evaluation  
Page 2

Appendix A - Photographs  
Geisinger Medical Center Abigail Pavilion  
Masonry Façade Evaluation  
Page 9



b.

c.

Figure 3.35: Masonry Preservation Services Report (2010) Roof Level: a) Wall section. b &c) Photographs of old building before renovation.



Figure 3.36: Roof Level Wall with Relief Angles Testing Grid

The Impact-Echo (IE) assessment method was conducted to investigate the characteristics and the conditions of selective locations in the masonry.

A backward calculation was performed to see if the wave speed for single wythe 10-celled brick masonry wall corresponded with a common wave speed. Figure 3.38 shows the use of the air coupled impact echo system to determine the p-wave speed of the brick in the wall. For single-Wythe masonry with mortar, the formula used by Sansalone and Strett for deriving the fundamental frequency was used to find the wave speed for the brick masonry. The average P-wave thickness frequency is  $f_t=5.58$  kHz for a single-wythe 10-cell cored brick wall. Since the brick used in this wall were 10-celled brick, there is a set percentage shift in the thickness frequency. The percentage shift in the thickness frequency,  $S = 0.22$  for 10 small circular cores. Using equation 3.2, the P-wave speed,  $f_t = 5.58$  kHz, so  $C_p = 1300$  m/s.

Table 3.2: Thickness frequency variables for single-wythe wall.

$C_p$	$\beta$	S	T	f
Brick	0.96	1.22	0.092 m	5.58 kHz

$$C_p = \frac{2 \times T \times S \times f}{\beta} \quad (\text{Eq. 3.2})$$



Figure 3.37: Single Wythe 10-celled brick wall.

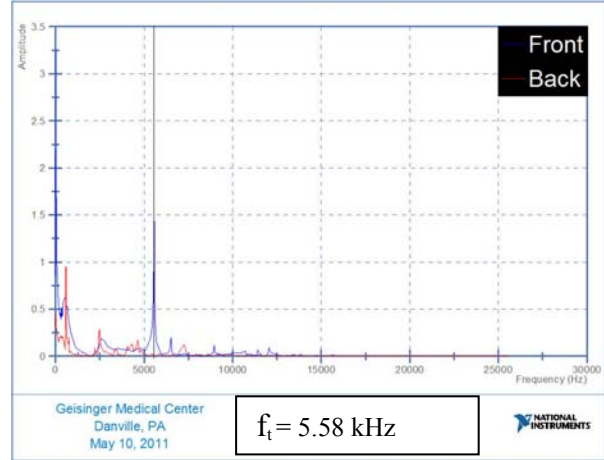


Figure 3.38: Impact echo response for single wythe 10-celled brick wall.

In addition, the thickness frequency was calculated for concrete masonry unit backup block with brick veneer as 4.78 kHz. Assumptions made for the P-wave speeds for: steel:6100 m/s, air is 332 m/s, gypsum 3200 m/s, block 3440 m/s, mortar is 3020 m/s, and grout is 3960 m/s.

The thickness frequency varies downward along the wall due to different construction. These calculated frequencies were found to match will with the experimentally determined frequencies

Table 3.3: Thickness frequency variables for various wall construction.

CMU	$\beta$	$C_p$	T	Gypsum Wall Board	$\beta$	$C_p$	T
Concrete Block	0.96	3440 m/s	0.092 m	Gypsum Wall Board	0.96	3200 m/s	0.0254 m
Air	0.96	3960 m/s	0.030 m	Steel Stud	0.96	6100 m/s	0.0015 m
Brick	0.96	1304 m/s	0.0920 m	Brick	0.96	1304 m/s	0.013 m
Mortar	0.96	3020 m/s	0.013 m	Mortar	0.96	3020 m/s	0.013 m
$f_t = 2.50$ kHz				$f_t = 5.78$ kHz			
CONCRETE BLOCK	$\beta$	$C_p$	T	Steel Angle	$\beta$	$C_p$	T
Concrete Block	0.96	3440 m/s	0.030 m	Concrete Block	0.96	3440 m/s	0.0127 m
Grout	0.96	3960 m/s	0.032 m	Brick	0.96	1304 m/s	0.092 m
Concrete Block	0.96	3440 m/s	0.030 m	Mortar	0.96	3020 m/s	0.013 m
Brick	0.96	1304 m/s	0.092 m	Steel Angle	0.96	6100 m/s	0.0079 m
Mortar	0.96	3020 m/s	0.013 m	Steel Stud	0.96	6100 m/s	0.0015 m
$f_t = 4.78$ kHz				$f_t = 5.97$ kHz			

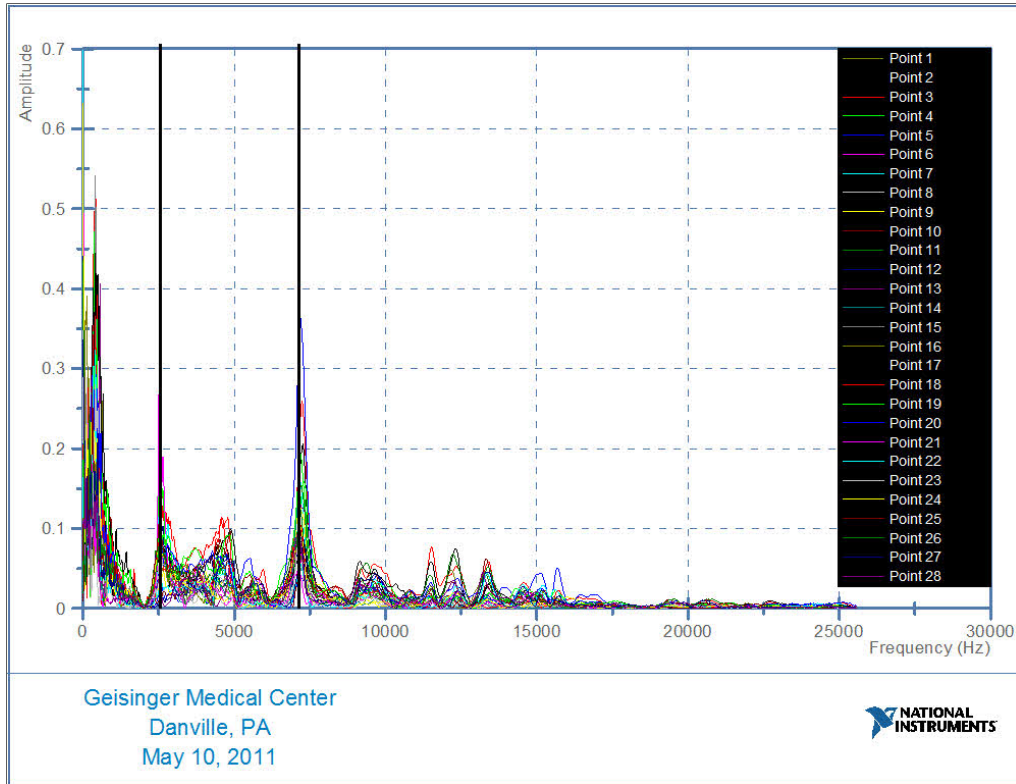


Figure 3.39: Impact echo responses for points 1 to 28. Peak 1 is at 2.5 kHz. Peak 2 is located at 7.1 kHz.

**3.2.1.2 Results:**

Using the Bonding Classification from Sadri (2003) in Figure 3.9 on page 42, the wall was classified as having poor bonding voids and poor bonding honeycombing. The results demonstrated that even with different materials, the air-coupled impact echo system was able to detect poor bonding between the brick veneer and back material. This area of the Geisinger Medical Center had not been renovated, so it was expected to detect poor bonding throughout the wall.

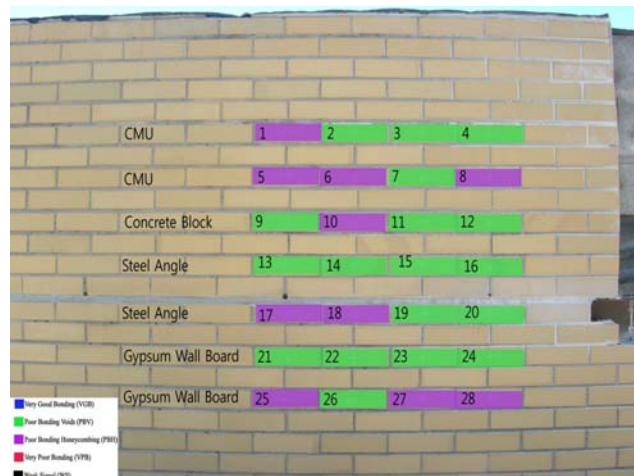


Figure 3.40: Geisinger Medical Center Test Results

## 4. Conclusions

It is concluded that the air-coupled impact echo method is a suitable alternative to displacement based impact-echo testing. The method offers a significantly easier placement and relocation of the transducer, and in many cases, especially for concrete slabs, the signals returned by the air-coupled system used in this study have obvious and very sharp peaks, facilitating the detection of the fundamental frequency of the slab

The testing of any point on a concrete slab or a masonry wall requires a prior estimation of the thickness frequency, according to the expected P-wave velocity in each of the components of the medium. Deviations of the observed fundamental frequency can be observed on the basis of the results of the testing. For concrete slabs, large shallow defects tend to produce a fundamental frequency below the thickness frequency, due to flexural modes of vibration in the delaminated area. Other defects produce an increase in the frequency, roughly inversely proportional to the depth of the defect divided by the thickness of the slab.

Contour plots of the lowest frequency over a grid of points provided a revealing way to visualize the results of the scan of a concrete slab. Choosing a spectrum where green represents approximately the thickness frequency allows the operator to distinguish between large, shallow defects, such as delaminations, which appear as a blue color, and deeper, smaller defects, which appear as a yellow, orange or red, depending on the depth. For the slabs tested and later cut open, these contour plots correlated reasonably well with observed unseen damage.

Scans of masonry walls are expected to indicate a number of response frequencies corresponding to the number of interfaces between mortar and units: thus, for a two wythe wall, a thickness frequency and two additional frequencies are expected, at roughly twice the thickness frequency. The presence of poor bonding between wythes can be detected by comparing the relative strength of each of these frequencies, using the templates given in Saadri (2003) and in this report for reference. The system proved reasonable effective in detecting areas of poor bond in laboratory specimens. The effectiveness of this system for masonry walls in the field needs to be more thoroughly tested

Some of the difficulties encountered with this system include the presence of spurious frequencies throughout some of the tests, which could not always be correlated to the thickness of the material. These may be the result of leaking noise from the impact, or lateral reflections of the P-wave in the medium under investigation. These signals can be removed manually or ignored in the development of the contour plots used for the investigation of the material

### 4.1 Range of Applicability of ACIE

In its present form ACIE has a clear applicability to the detection of defects in historic masonry and concrete. However, there are also some very clear limits on the applicability of this method. In concrete, the principal limitation on the ACIE method is the depth of the concrete specimen being examined. Larger depth creates problems both in the ability to generate a sufficient impact and in the ability to interpret the return signal, as larger impactors can only detect large defects. Based on the system used in this study, the size of the ball, either a hand held spring ball or a ball

powered by compressed air, is approximately 2 cm, that is a little over 3/4" inch in diameter. The use of a ball this size is required to obtain a readable signal in a wall, slab, beam, or column 50-75 cm (18"-24") thick. As such, this places a limit on the usability of this equipment for investigations of concrete structures over 50 cm in thickness. For larger or thicker structures, through transmission methods or ground-penetrating radar may be preferred. However, ACIE remains a very useful method for the investigation of most concrete slabs or walls.

The investigation of masonry walls, and horizontal masonry structures such as vaults or domes requires significant operator knowledge about the masonry construction practices prevailing at the time of construction, and about masonry techniques in general. The investigation of masonry structures requires a great many subjective judgments to be made in choosing impactors, reviewing the character of the signals, in order to obtain a meaningful result. It is significantly more difficult to establish arbitrary limits on the applicability of this method. In this study, it has been used successfully on three-wythe brick masonry walls and vaults with a thickness of 30-45 cm. It appears that the limits can be extended 50 cm and beyond in thickness without appreciable difficulty, except that locating interfaces between wythes would become increasingly difficult. The lower velocity signal in masonry allows smaller defects to be identified, even using larger sizes of impactors to excite vibrations. This method is best used transverse to the wall thickness and appears to be applicable up to a thickness of 50-75 cm. Beyond this thickness, again, transmission methods and ground-penetrating radar may be preferred.

#### **4.2 Special Instructions/Cautions in the Application of Air-Coupled Impact Echo**

A significant advantage of the air-coupled method of impact-echo analysis is the clarity of the peaks in the frequency plot, due to the reliance on reading the untransformed magnitude of the frequency response, rather than the RMS intensity of the response. The result is a series of very sharp peaks at distinct frequencies. In many cases, as seen above, each of these peaks can be identified, as the series of mortar/unit interfaces in a masonry wall. This allows the operator to discriminate between intact mortar joints and missing mortar joints or joints with defects. However, occasionally other frequencies are introduced, and repeatable throughout the test of a wall or other specimen that cannot be correlated to any physical feature of the wall or slab. During the testing reported in this study, this occurred most frequently at frequencies well below the thickness frequency, but, on some occasions also occurred at intermediate frequencies. It is necessary to recognize these spurious frequencies and to discard them in completing the analysis and interpretation of the results of the testing. Examples are given above in the testing program on tunnel slabs and in some of the wall tests reported above.

## 5. Acknowledgments

The authors are especially grateful to Erik Valentino of Masonry Preservation Systems, Inc. for access to project sites and for the donation of materials, labor, and warehouse space for the construction of the masonry experimental specimens used in this project.

The authors thank Hiroki Ota and Jim Chavanic for assistance with the laboratory portion of the concrete slab study. The authors further acknowledge the Office of Physical Plant at Penn State University, notably Chris Musser, Al Matyasovsky, Ed Gannon, and Steve Maruszewski, for cooperation in making the utility tunnel project available, and for making space for storage of removed tunnel cover slabs, and for assistance in the forensic program on these slabs. The authors also acknowledge the cooperation of Joe Wernert at G.M. McCrossin assistance with and access to the slabs during construction.

## 6. References Cited

ASTM C1383–04. (2010). “Standard Test Method for Measuring the P-Wave Speed and the Thickness of Concrete Plates Using the Impact-Echo Method”. ASTM International, West Conshohocken, PA, 2003. DOI: 10.1520/C1383-04R10.

Berriman, J., Hutchins, D., Neild, A., Gan, T., and Purnell, P. (2006). “The application of timefrequency analysis to the air-coupled ultrasonic testing of concrete”. *IEEE Transaction on Ultrasonic, Ferroelectrics and Frequency control*, Vol. 53, Issue 4, 768 – 776

Boothby, T., Atamturktur, S., Kremer, P., Pistone, E., and Trujillo, N. (2010). *Assessment of Historic Concrete and Masonry by Broadband Vibration Testing*. Strategic Environmental Research and Development Program (SERDP).  
<<http://serdp.org/content/download/8545/104680/file/RC-1653-FR.pdf>>

Büyüköztürk, O. (1998). “Imaging of Concrete Structures”. *NDT&E International*. Vol. 31, Issue 4, 233-243.

Carino, N. (2011). “Training: Often the Missing Link in Using NDT Methods”. *Construction and Building Materials*. doi:10.1016/j.conbuildmat.2011.03.060

Chen, B., Wang, J., Wang, H., Chang, T., and Yang, Z. (2009). “Effect of Void Ratio of Concrete on Evaluation of P-wave Velocity by Impact-echo Method”. *International Journal of Applied Science and Engineering*. Vol. 6, Issue 3, 199-205.

Erdly, J. (2010). *Masonry Façade Evaluation Geisinger Medical Center Abigail Pavilion*. Rep. no. MPS Project No.: 200954. Masonry Preservations Services.

Gibson, A., and Popovics, J. (2005). “Lamb Wave Basis for Impact-Echo Method Analysis”. *Journal of Engineering Mechanics*. Vol. 131, Issue 4, 438 – 443.

Kesner, K., Sansalone, M., and Poston, R. (2004). “Use of the Impact-Echo Method to Evaluate Damage due to Distributed Cracking in Concrete Plate Members: Theory and Field Trials”. *Transportation Research Record: Journal of the Transportation Research Board*. Vol. 1893. 61 – 69.

Krautkrämer, J. and Krautkrämer, H. (1990). *Ultrasonic Testing of Materials* (4th Ed). Springer-Verlag. New York, NY, USA

Riewestahl, Brian. (2011). *Evaluation of Concrete Slabs Using Automated Air-coupled Impact – echo Method*, M.S. Thesis, The Pennsylvania State University.

Sadri, A. (2003). “Application of impact-echo technique in diagnoses and repair of stone masonry structures”. *NDT&E International*. Vol. 36, Issue 4, 195 – 202.

Sansalone, M. and Streett, W. (1997). *Impact-Echo – Nondestructive Evaluation of Concrete and Masonry*. Bullbrier Press, Jersey Shore, PA, USA.

Santamarina, J., Klein, K., and Fam, M. (2001), *Soils and Waves*. John Wiley & Sons Ltd. Chichester, West Sussex, England

Smith, S. (1997). *The Scientist and Engineer's Guide to Digital Signal Processing*. California Technical Publishing. San Diego, CA, USA.

Zhu, J. and Popovics, J. (2005). “Non-contact imaging for surface-opening cracks in concrete with air-coupled sensors”. *Materials and Structures*. Vol. 38, Issue 283, 801 - 806.

Zhu, J. and Popovics, J. (2007). “Imaging Concrete Structures Using Air-Coupled Impact-Echo”. *Journal of Engineering Mechanics*. Vol. 133, Issue 6, 628 - 640.